January 2015

Development and Characterization of hybrid thermoplastic composites

Priyanka C. Karkhanis
Purdue University

Graduate School Form 30
Updated 1/15/2015

PURDUE UNIVERSITY
GRADUATE SCHOOL
Thesis/Dissertation Acceptance

This is to certify that the thesis/dissertation prepared

By Priyanka Chandrashekhar Karkhanis

Entitled Development and Characterization of Hybrid Thermoplastic Composites

For the degree of Master of Science in Aeronautics and Astronautics

Is approved by the final examining committee:

Byron Pipes
Chair

Vikas Tomar

Chin-Teh Sun

To the best of my knowledge and as understood by the student in the Thesis/Dissertation Agreement, Publication Delay, and Certification Disclaimer (Graduate School Form 32), this thesis/dissertation adheres to the provisions of Purdue University's "Policy of Integrity in Research" and the use of copyright material.

Approved by Major Professor(s): Byron Pipes

Approved by: Weinong Chen 11/23/2015
Head of the Departmental Graduate Program Date

DEVELOPMENT AND CHARACTERIZATION OF HYBRID THERMOPLASTIC COMPOSITES

A Thesis

Submitted to the Faculty

of

Purdue University

by

Priyanka Chandrashekhar Karkhanis

In Partial Fulfillment of the

Requirements for the Degree

of

Master of Science in Aeronautics and Astronautics

December 2015

Purdue University

West Lafayette, Indiana

Dedicated to my Dad, my hero and my inspiration.

ACKNOWLEDGEMENTS

I would like to extend my deepest gratitude and appreciation for the help and support to the following people who have in one way or the other contributed to make this study possible.

To Dr Byron Pipes, for introducing me to the inner workings of composites, his support, guidance and direction that helped me take up this project and successfully complete it. Without his faith and support, this project would not have been possible.

To Dr Hans Luinge, for giving me the opportunity to work on this project and for constant guidance and help during this research. To all the employees at TenCate, for helping me throughout the project.

To Dr Laurent Warnet, for guiding me throughout this project and having faith in me. To University of Twente, for allowing me the access to their testing facility.

To all my colleagues at Purdue University for helping me through my research.

To Mr Jayneel Gajjar for his constant support and motivation to work harder.

Finally to my parents, Mr Chandrashekhar Karkhanis and Mrs Pradnya Karkhanis for their support, their faith in me and for their guidance. You will always be my inspiration.

TABLE OF CONTENTS

Page

LIST OF TABLES i

LIST OF FIGURES viii

ABSTRACT x

CHAPTER 1. INTRODUCTION 1

1.1 Background 1

1.2 Polyphenylene Sulfide 5

1.3 Cetex © by TenCate Advanced Composites 7

1.4 'Clips' in aerospace industry 11

1.5 Hybrid Composites 12

CHAPTER 2. MECHANICAL PROPERTIES 16

2.1 Flexural Strength 16

2.2 Interlaminar Strength 24

2.3 Bearing Strength 28

CHAPTER 3. MATERIALS 33

3.1 Honeycomb Structures 34

3.2 Foams 34

3.3 Glass and Discontinuous carbon-PPS flakes 35

CHAPTER 4. MANUFACTURE OF LAMINATES 37

4.1 Flat Laminates 37

4.2 Press Cycle 39

4.3 C-scans 41

4.4 V-shape laminates 43

4.5 Press cycle for thermoforming 44

Page

CHAPTER 5. TESTING 48
5.1 Three point bend test 48
5.2 Four point bend test for a curved beam 50
5.3 Double Lap Shear test 53
CHAPTER 6. ANALYSIS 57
6.1 Flexural strength 57
6.2 Interlaminar strength 63
6.3 Bearing strength 65
CHAPTER 7. MICROSCOPY 70
7.1 Sample Preparation 70
7.2 Failure pattern in flexural test samples 71
7.3 Failure pattern in interlaminar strength test samples 73
7.4 Failure pattern in bearing test samples 75
7.5 C-scans 81
CHAPTER 8. CONCLUSION 84
CHAPTER 9. FUTURE RESEARCH 86
LIST OF REFERENCES 90

LIST OF TABLES

Table Page

1-1 Comparison of properties for different thermoplastic resin 5

1-2 Physical properties of PPS resin 6

1-3 Neat resin Properties 6

1-4 Ply properties of Cetex © carbon-PPS 8

1-5 Ply properties of Cetex © glass-PPS 9

3-1 Specifications for materials used in the research 36

4-1 Volume fractions of the different constituents in laminates 43

4-2 Volume fraction in legs and curvature of the sample 46

5-1 Sample and setup dimensions at TenCate Advanced Composites testing facility 49

5-2 Test setup dimensions 51

5-3 Test sample geometry 55

6-1 Comparison of different laminates and their bending compliances 59

6-2 Specific flexural strength and flexural modulus for different laminates 60

6-3 Comparison on flexural modulus values obtained analytically vs experimentally 61

6-4 Interlaminar strength and coefficient of variation for different laminates 63

6-5 Initial bearing strength and specific bearing strength for different laminates 66

6-6 Ultimate bearing strength and specific bearing strength 66

7-1 Different samples and respective initial bearing strength 82

9-1 Flexure test data for carbon-PPS and hybrid 3 88

LIST OF FIGURES

Figure Page

1-1 Forecasted Thermoplastic composites flyaway requirements by market segment..... 1

1-2 Thermoplastic composites in commercial aircrafts: A timeline..... 3

1-3 Comparison of selected aerospace thermoset and thermoplastic resin matrices..... 4

1-4 Chemical Structure of PolyPhenylene-Sulfide..... 6

2-1 Coordinate system for single ply..... 18

2-2 Global coordiinate system applied to the laminate..... 18

2-3 Ply wise stresses in terms of material properties, strains and curvatures. 20

2-4 Laminate Structure with ply numbers and distances..... 20

2-5 Different modes of failure for a bolted sample..... 29

3-1 Phenolic and Aluminium honeycomb structures..... 34

3-2 High temperature foams 35

3-3 Glass fabric and discontinuous carbon-PPS flakes..... 35

4-1 Laminate layup and ply numbers 37

4-2 Hybrid 2 during layup and final consolidated laminate 38

4-3 Hybrid 3 Discontinuous carbon-PPS flakes 39

4-4 Hybrid 3 during layup and fully consolidated laminate 39

4-5 Hot press at TenCate and Upilex release fims with thermocouple..... 40

4-6 Temperature profile in the hot press..... 41

4-7 C-scans of different laminates 42

4-8 Schematic of the thermoforming process flow..... 44

4-9 Thermoforming facility at TPRC, Netherlands 45

4-10 Laminate after thermoforming..... 45

4-11 Samples made after cutting using diamond saw..... 45

Figure Page

4-12 Test sample 46
5-1 Free body diagram for the setup and sample in three point bending 48
5-2 Test samples for carbon-PPS laminates 49
5-3 Test facility at TenCate Advanced Composites 49
5-4 Free body diagram of test sample and test setup 50
5-5 Test sample for four point bend test 52
5-6 Test setup and LVDT at University of Twente 52
5-7 Test sample geometry 54
5-8 Clamped section on bearing specimen 55
5-9 Test setup at TenCate and loading plates 55
5-10 Bearing samples 56
6-1 Input parameters for LAP software 58
6-2 Output given by the LAP software 58
6-3 Load vs displacement graph for all the laminates 62
6-4 Force vs displacement for different laminates 64
6-5 Fiber bridging and buckling for bearing failure 68
6-6 Bearing strength vs displacement in different laminates 68
7-1 Epoxy-Hardener system and samples cured in the mixture 70
7-2 Automatic Polisher (Bubhler vector and pheonix alpha grinder) 70
7-3 Olympus microscope couples with Sony video camera system 71
7-4 Carbon-PPS before and after the test 72
7-5 Failure in Hybrid 1 and Hybrid 2 72
7-6 Failure in Hybrid 3 and glass-PPS laminate 73
7-7 Carbon-PPS laminate after failure 74
7-8 Failure in hybrid 1 and hybrid 2 74
7-9 Failure in hybrid 3 and glass-PPS 74
7-10 Constrained region on laminate and bearing plane in a sample 76
7-11 Hole circumference observed under microscope 77

Figure Page

7-12 Circumference region for carbon-PPS and hybrid 1 77
7-13 Circumference region for hybrid 2 and hybrid 3 77
7-14 Location of microscopic images 78
7-15 Initial peak for carbon-PPS and hybrid 1 78
7-16 Initial peak for hybrid 2 and hybrid 3 78
7-17 Damage at ultimate load in carbon-PPS at the hole edge and at washer edge 79
7-18 Ultimate failure in hybrid 1 and hybrid 2 80
7-19 Ultimate failure in hybrid 3 80
7-20 C-scans of bearing test samples showing flake distribution 81
7-21Thickness scale for samples 1-5 and thickness scale for sample 6 81
9-1 Carbon-PPS and hybrid 3 laminate at Purdue University 86
9-2 Hot press and flat mold at Purdue University 86
9-3 Load vs displacement for carbon-PPS and hybrid 3 87
9-4 Electrical circuits for the thermoforming system 89
9-5 V-shape mold for angle parts 89

ABSTRACT

Karkhanis, Priyanka, C. M.S., Purdue University, December 2015. Development and Characterization of Hybrid Thermoplastic composites. Major Professor: Byron Pipes.

This work is aimed at studying the possibility of using interply hybrid woven thermoplastic semi-pregs in secondary structures in aircrafts at TenCate Advanced Composites, Netherlands and Purdue University. Three different interply hybrids were designed from combination of Cetex © carbon-PPS semi-preg, Owen corning's woven glass with PPS sheets and discontinuous chopped Cetex © carbon-PPS semi-preg to get desired flexural, out of plane and bearing properties. The design calculations are done based on classical laminate theory and the selection of materials to be used with carbon-PPS was done based on cost and availability. The Hybrid laminate performances are analyzed and compared to the conventional Cetex © Carbon-PPS semi-preg laminates. Observations are reported on three point bend test (European standard 2562), four point bend test(ASTM D6415-99) and bearing test (Airbus standards AITM 1-0009) for the laminates and it was found that hybrid laminates show a reduction of 5-10% in bending stiffness, 20-40% reduction in out-of-plane strength and 2-5%reduction in bearing with a cost reduction of 20-30%. The research identifies and documents the different factors responsible for failures and reduction in strength in the Hybrids.

CHAPTER 1. INTRODUCTION

1.1 Background

Fiber reinforced thermoplastics have been used in the aeronautics industry since 1980's. They entered the market late due to higher costs and lack of processing techniques in early days. However due to development of low cost manufacturing techniques developed by 1980, acceptance of fiber reinforced thermoplastic composites into the mainstream aerospace structures has increased. Since 1990's fiber reinforced thermoplastic composites have been used in several aeronautics areas like thermoplastic skins reinforced with welded ribs in A340-600 and A380, ribs in ailerons, angle brackets and panels for the leading edges of A340-600, floor panels for Gulfstream's G450, G550 and G650 and a huge number of carbon fiber/PPS clips and cleats used to secure exterior skins to their circular frame sections. Thermoplastics have been used in military applications as well. Cargo floors of Sikorsky Aircraft's CH-53K are some of the largest thermoplastic parts ever to be used on the aircraft [1].

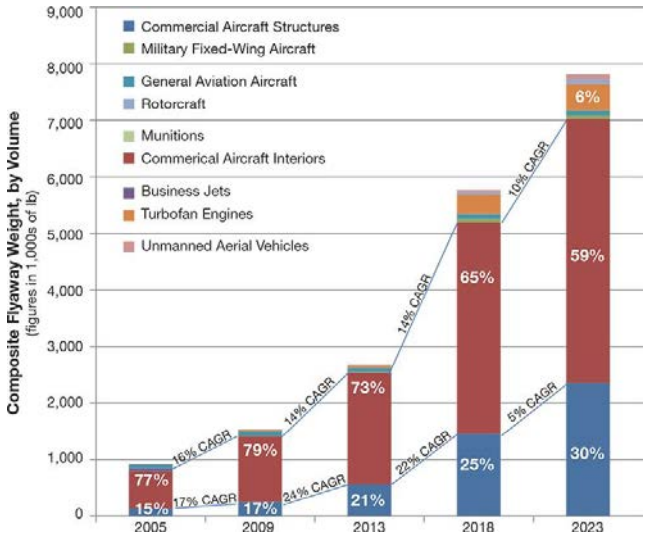

Fig 1-1 Forecasted Thermoplastic composites flyaway requirements by market segment.

Although thermoplastic composites have been in use for more than 30 years, they are coming into the main stream recently. Only in the past 10 years, the thermoplastic composites have gained momentum and have applications that can be considered large and high volume [1]. They have been growing not only in the aerospace industry but also into the automotive, medical, marine and sports with the initial driving point being higher impact resistance and inherent flame resistance. The thermoplastic market has experienced a significant growth in the last 5 years with an expected forecast of 12% increase in the next 5 years [2] as seen in the fig 1-1. They are mainly used in aerospace industry as leading edges, interior components, access doors, engine pylons and other variety of parts.

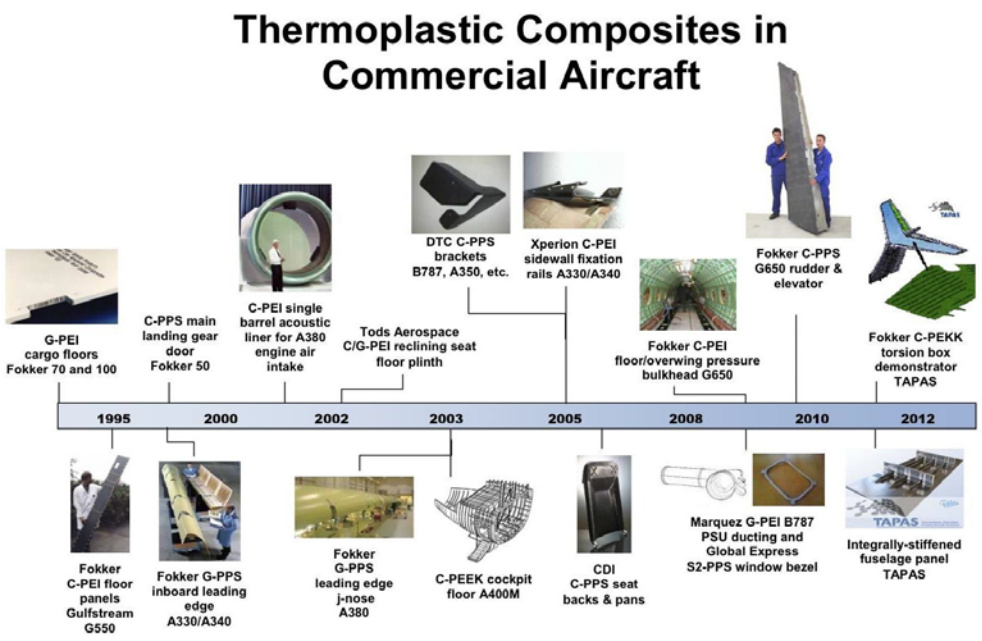

Fig 1-2 Thermoplastic composites in commercial aircraft: A timeline

As compared to thermosets, thermoplastic composites do not need to be cured. Instead they need to be 'consolidated' under high temperature and pressure to make a part. A thermoplastic composite can be re-heated and reformed above its softening temperature. This characteristic enables the manufacturers to establish faster cycle times as compared to thermosets which takes time to cure and cannot be re-shaped once cured. Thermosets are needed to be stored at low temperatures to prevent the slow polymerization which would harden the resin and render it useless for forming. However since thermoplastics can be melted they need not be stored at low temperature thus eliminating the need of freezers. Fig 1-3 shows a comparison between the continuous service temperature, cure time and tensile strength of thermosets and thermoplastics. Usually the thermosets have curing rates in range of an hour to several hours as compared to the consolidation time of minutes for the thermoplastics. The thermoplastics also show significantly higher tensile

modulus as compared to thermosets. Due to this paradigm shift towards the process/cost efficiency, reinforced thermoplastics now appear to be on their way of capturing a bigger market share in the aerospace industry [3].

Resin Family	Continuous Service Temp. (°C / °F)	Cure Time (min)	Tensile Strength (ksi)	Tensile Modulus (Msi)
Thermoset Resins				
Phenolic (PH)	170 / 340	60+	6.9	0.55
Epoxy (E)	180 / 350	60-240	9.7	0.34
Cyanate ester (CE)	180 / 350	60-180	7.4 - 13.2	0.38 - 0.45
Bismaleimide (BMI)	230 / 450	120 - 240+	10.5	3.9
Polyimide (PI)	370 / 700	120+	16.6	-
Thermoplastic Resins				
Polycarbonate (PC)	120 / 250	< 20	9.4	0.33
Polyphenylene sulfide (PPS)	240 / 464		13.5	0.5
Polyetherimide (PEI)	200 / 390		6	0.8
Polyetheretherketone (PEEK)	250 / 480		14 - 33	0.58 - 3.4

Fig 1-3 Comparison of selected aerospace thermoset and thermoplastic resin matrices.

Thermoplastics have been used to make some of the biggest composites parts in aerospace. An example can be given of Westland Helicopters who made a 3 meter long main body of horizontal tailplane comprising of four panels joined together by thermos-fusing under pressure [4]. The material used for manufacturing was provided by Dutch specialist TenCate Advanced Composites. The Gulfstream Aerospace G650 has thermoplastic rudder and elevator which are some of the biggest parts on an aircraft.

The first thermoplastic resin to be tried in the aerospace industry was PEEK. By 2000, polyetherimide PEI was applied in the structural parts. However it had a disadvantage of being extremely sensitive to aggressive fluids commonly used in the aircraft industry [4].

Some of the other thermoplastic resins in use are polycarbonates(PC), polyamides(nylon, PA-6,PA-12), polyphenylene sulfide (PPS), polyetherketoneketone(PEKK) [1]. Table1-1, obtained from a report presented by Fokker Aerospace, summarizes comparison between different thermoplastics depending on their properties.

Table 1-1 Comparison of properties for different thermoplastic resins

	Mechanical Properties	Cost	Processing temperature	Tg	Chemical resistance	Bonding
PEEK	++	-	0	+	+	-
PEI	+	+	+	+	-	+
PPS	+	+	+	0	+	-
PEKK	++	0	0	+	+	+

1.2 Polyphenylene Sulfide (PPS)

The selection of a thermoplastic resin is done based on the properties required for an application. For this research, polyphenylene sulfide was selected as the thermoplastic resin based on its mechanical properties. Polyphenylene Sulfide (PPS) is an organic polymer consisting of aromatic rings linked with sulfides (C_6H_4S). It is semi-crystalline in nature having symmetrical, rigid backbone chain and was developed by Philips Petroleum in 1968 [5]. PPS shows good resistance to nearly all the solvents present. It is impossible to dissolve in any acid below 200°C. Due to the low Tg (90°C) of PPS because of flexible sulfide linkage between the aromatic rings [6], it is highly suitable to be used in the aerospace industry.

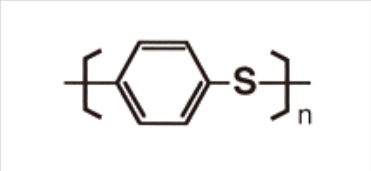

Fig 1-4 Chemical structure of PolyPhenylene-Sulfide

Fortron is one of the key manufacturer of PPS resin. PPS is mostly used in applications where the structure is under load for extended periods of time as high percentage of matrix maintain its crystallinity even above its Tg and hence gives excellent performance. The thermal degradation of PPS starts at temperature of 370°C. The physical properties of PPS obtained from the material safety document sheet by TenCate are given in the table 1-2.

Table 1-2 Physical properties of PPS resin

Property	Temperature
Shelf Life	Indefinitely below 40°C
Shop Life	Indefinitely below 40°C

Table 1-3 Neat Resin Properties

Property	Values
Tg	90°C
Specific Gravity	1.35
Melt temperature (Tm)	280°C

Property	Value
Tensile properties Tensile Strength Tensile modulus Elongation	 90.3 MPa 3.8 MPa 3% (at yield)
Thermal properties Thermal conductivity Coefficient of thermal expansion (CTE)	 0.19 W/m-°K 52.2 ppm/°C
Poission's ratio	0.36

1.3 Cetex © by TenCate Advanced Composites

TenCate Advanced Composites is a leader in the thermoplastic technology [7]. The company markets fiber based pre-pregs combining carbon, glass and aramid with PEEK, PEI and PPS. The Cetex © PPS developed by TenCate is a reinforced semi-crystalline polyphenylene sulfide thermoplastic composite consisting of woven fabric like carbon and glass, coated with thermoplastic resin. The material exceeds 35/35 OSU and is qualified at Airbus and Boeing for multiple structural applications.

The woven fabric increases the drapability and can take flexural and tensile load in multiple axes and show good off-axis stiffness properties. The bending of the fiber during weaving results in loss of strength and stiffness. However if the fibers are broken in a particular region, the surrounding fibers behave as unbroken due to their weave. The strength and stiffness of the material not only depends on the matrix and the fiber

properties but also on the fabric count and weave style. The weave determines how the warp and weft yarns are interlaced [8].

The Cetex © comprises of carbon fabric in 5-harness satin weave where the fiber bundles traverse in both warp and weft direction changing over/under positions. The satin weave have less crimp than plain weave, which give better mechanical properties and have same fiber strand count in warp and weft directions [9]. However the satin weave is asymmetrical resulting in fiber running predominantly in the warp direction while the other face has fiber running in the weft direction [10]. This asymmetric effect can be overcome by making a symmetrical layup while manufacturing the laminate.

The mechanical properties of Cetex © material used in this research are given in the table 1-4. The data has been taken from the Cetex © datasheet provided by TenCate Advanced Composites. Cetex © consists of T300 carbon fibers with 3K fibers per bundle and a double sided coating of PPS film. The properties are measured at 23°C with 50% relative humidity.

Table 1-4 Ply properties of Cetex © carbon-PPS

Property	Values
Mass of fabric+ resin	486 g/m2
Ply thickness	0.31mm
Tensile properties Tensile Strength (warp)	758 MPa

Property	Value
Tensile modulus (warp)	56 GPa
Tensile (weft)	54 GPa
Compression properties	
Compressive strength (warp)	644 MPa
Compressive modulus (warp)	51 GPa
Compressive modulus	51 GPa
Shear properties	
In-plane shear strength	119 MPa
In-plane shear modulus	4.04 GPa
Bearing properties	
Bearing strength (yield)	454 MPa
Bearing strength (ultimate)	844 MPa

TenCate also markets woven glass-PPS semi-preg under the Cetex © brand. The glass fabric in glass-PPS semi-preg is 8 harness satin weave (US7781 fabric style) with PPS matrix system. The mechanical properties for glass-PPS semi-preg are given in table 1-5.

Table 1-5 Ply properties for Cetex © Glass-PPS

Property	Value
Mass of fabric+resin	475 g/m^2
Ply thickness	0.25 mm
Property	Value

Tensile properties	
Tensile Strength (warp)	340 MPa
Tensile modulus (warp)	22 GPa
Tensile modulus (weft)	20 GPa
Compression properties	
Compressive strength (warp)	425 MPa
Compressive modulus (warp)	26 GPa
Compressive modulus (weft)	24 GPa
Shear properties	
In-plane shear strength	80 MPa
In-plane shear modulus	3.714 GPa
Bearing properties	
Bearing strength (yield)	318 MPa
Bearing strength (ultimate)	516 MPa

The other type of fabric used is the plain glass fabric. The fabric has 2*2 twill weave and higher filament diameter than glass-PPS semi-preg which makes this fiber thicker. The fabric shows similar properties as glass-PPS semi-preg However as this fabric is not reinforced with the PPS resin, it becomes necessary to add sheets of PPS resin in the laminate while manufacturing.

1.4 ‘Clips’ in aerospace industry

Boeing 787 and Airbus A350 both have used extensive amount of thermoplastic composites in recent times. For B787, to keep the weight low and performance high, Boeing adopted one-piece fuselage barrels. Airbus on other hand has five major fuselage sections with four large shells or panels. Each panel is supported by a system of internal frames and stringers. The stringers are bonded directly to the skin panels, but an array of parts called ‘clips’, attach the frames to the skin. According to the Premium Aerotec, they design more than 3000 clips for different parts of the aircraft. Due to the huge number of part requirement for a single aircraft, the clips need to have very short manufacturing cycle, low labor demand and a great deal of flexibility. For these reasons, thermoplastic matrix composites are found to be most suitable for the structure [11]. The clip dimensions range from approximately 100mm upto 800mm in length and from 30mm to 40mm in width.

To meet the performance criteria, Premium Aerotec uses intermediate carbon fiber in PPS resin. TenCate is one of the major suppliers of material for the manufacture of this ‘clip’. The clip laminates have quasi-isotropic layup and are supplied in different thicknesses ranging from 1mm to 5mm or 5 to 14 pre-preg plies. The thickness of the clips keep varying according to the changing load conditions [11]. Due to the higher production rates, it becomes necessary to reduce the manufacturing cost of the clips while retaining the mechanical properties and physical strength. This brings up the need to experiment with different combinations of fiber systems available currently to develop materials which give higher or similar mechanical properties as the original laminate

structure. The aim of this research was to develop combination of materials to give similar properties as the all carbon-PPS layup for the clip structure at TenCate.

1.5 Hybrid Composites

The term ‘Hybrid composites’ is used to define a laminate having atleast two types of fiber reinforcements in a single resin system. The behavior of a ‘hybrid composite’ can be considered as an average of the individual components in which there is more favorable balance between the inherent advantages and disadvantages. Hybrid composites are generally used to complement the limitation of a single fiber system using other fiber system. However predicting their properties becomes difficult due to complex interaction between the fiber systems [12]. According to Kretsis, hybrid composites are classified based on how the different fiber systems are mixed. The different classifications in composites are sandwich structures, tow-by-tow hybrids, interply hybrids and intimately mixed with fibers mixed in random fashion [13].

Tow-by-tow hybrids consists of different fiber systems weaves together and coated with a single matrix. Intimately mixed hybrids consists of different mixed together to avoid over concentration of any one type of fiber system in the laminate. A disadvantage of these hybrids is that predicting their properties become difficult.

Sandwich hybrids consists of two thin but stiff skins attached to the core material using adhesives. This type of structures give excellent stiffness and strength with lowest overall density. Thicker is the core, higher is the flexural stiffness of the structure. The skins

provide the required in-plane shear stiffness, bending stiffness and carry axial and in-plane shear loading. The core material provides spacing between the skins thus increasing the flexural stiffness of the structure and reduces the weight of the overall structure. This makes them an attractive option to be used in many aircraft panels. The most popular core used is Nomex © which is manufactured from aramid paper, shaped into honeycomb, hexagonal cell structures and dipped in phenolic resin to improve the mechanical properties and gain some stability. Other core materials in use are aluminium, titanium, fiberglass etc. However the sandwich structures have poor in-plane strength and through thickness strength. In sandwich structure, the face sheets or skins are attached to the core with adhesive which transfer the shear load from core to the skin. This adhesive layer becomes a failure point as it becomes the non-reinforced layer in the entire structure. Therefore higher factor of safety becomes necessary while designing the structure.

Interply hybrids are similar to sandwich structures and are formed by placing plies of different fibers in a structured manner and specific orientation to obtain desired properties. The honeycomb core structure is replaced with fiber plies. For the interply hybrids, placement of the plies in the laminate structure becomes critical and affects the properties of the entire laminate. Kalnin [14] found that flexural modulus is greatly affected by percentage of graphite plies in the all glass reinforcement and its placement from the center of the laminate. He concluded that the large increase in flexural stiffness is seen with small addition of graphite and can be called as the hybridization effect of combining two fiber systems. Kretsis [13] studied the hybrid effect in carbon-glass epoxy laminates in the tensile, compressive and flexural properties of the laminates. According to a study

done by Zhang et al [15], the interply carbon glass hybrid laminates with 50% carbon fiber reinforcement provide the best flexural properties when the carbon layers are placed at the exteriors. The tensile strength was found unresponsive to the stacking sequence but depends on the percentage of carbon in the glass laminates.

Another type of interply hybrid can be made using the random discontinuous long fiber reinforced thermoplastics (carbon-PPS flakes) in addition to the carbon reinforced thermoplastics. Many companies liked Hexcel, Boeing and Northrop Grumman [16] have started researching the possibility of using aligned discontinuous long fiber thermosets. The use of random discontinuous carbon-PPS flakes is relatively new to the aerospace field and consists of compression molding of discontinuous carbon-PPS flakes to form parts. Like other thermoplastics, the discontinuous carbon-PPS flakes require higher temperatures than many thermosets and higher degree of temperature control during cool down. However due to long fibers, the parts made have a higher mechanical properties than the short fiber parts made by injection molding materials [17]. Pressing the discontinuous carbon-PPS flakes together with woven carbon reinforced thermoplastic creates a new hybrid with properties almost equivalent to the CFRP laminates. The properties of Discontinuous carbon-PPS flakes have not been researched extensively and hence its usage in aerospace is limited.

Three different hybrids were created and researched as potential materials for the ‘clip structure’.

a) Woven carbon reinforced PPS combined with twill weave glass fabric.

b) Woven carbon reinforced PPS combined with woven glass reinforced PPS semi-preg.

c) Woven carbon reinforced PPS combined with woven discontinuous long fiber reinforced thermoplastics.

The research also investigates the flexural, inter-laminar and bearing strength of these hybrids and tries to explain the variation in the properties of the hybrids. The mechanisms behind these properties and their variation in the hybrids are explained in the chapter 2.

CHAPTER 2. MECHANICAL PROPERTIES

2.1 Flexural Strength

The use of hybrids to increase the flexural toughness is not new and has been investigated before. Researchers have tried to use carbon-glass hybrids to increase the flexural stiffness of an all carbon structure. Stevanovic et al [18] researched the flexural, tensile and impact behavior of carbon-glass hybrid fiber reinforced polyester composites. He found that the flexural modulus of the hybrids exceeded that of the full carbon laminates due to the higher contribution of the outer carbon fiber reinforced layers. Chensong Davis et al [19] investigated the effect of using different types of glass fibers in combination with unidirectional carbon fiber on the flexural strength of the laminate structure. The research was primarily directed in replacing the carbon layers on the surface with varying degree of glass fibers and it was found that flexural strength decreases with increasing percentage of glass fibers on the surface of the carbon laminate with all types of glass fibers.

Woven hybrids are relatively new in this field. Zhang et al [15] investigated the possibility of using woven carbon-glass fabric hybrids for application in lightweight load bearing structures. They used plain weave glass fabric in combination with twill weave carbon fabric with epoxy system to make multiple inter-ply laminates with glass

fabric in different positions with respect to the mid plane. They found that by placing two carbon plies at the exterior effectively increased the flexural strength as compared to placing carbon plies elsewhere within the laminate structure.

The flexural stiffness of a material is defined as the resistance of a structure against bending deformation and is dependent on elastic modulus and area moment of inertia. For the structure under focus, bending stiffness is one of the critical properties from design point of view. Applying the Hook's law to composite laminates on a macro scale, the strain stress relationship can be expressed can be expressed as $\{\epsilon\}=[S]*\{\sigma\}$, where [S] is the matrix for material compliance and depends on the fiber and matrix properties. In this research, classical laminate theory (CLT) is used to estimate the flexural stiffness of the laminate and the results are compared to the experimental data.

In woven fabrics, the principle directions can be defined as '1' for the warp direction, '2' for the weft direction and '3' is normal to the plane of the laminate. Four basic ply material properties are necessary for the analysis using the CLT (E_{11}, E_{22}, ν_{12} and G_{12}). These properties can be found through experiments or using micromechanics theories for woven fabric. According to the research done by Akkerman [21], these analyses consider a geometric model which represents different regions in a representative volume element (RVE) like impregnated warp bundle, impregnated weft bundles and resin along with fiber volume fraction and weave type. The bundle properties are predicted using the classical micromechanics equations and then are transformed in a laminate co-ordinate system. The final properties are found by averaging the properties found from different

fiber bundles and assuming uniform state of strain [20]. U200MM, MMTEXLAM and WISETEX are some of the softwares used to predict the woven fabric properties. TenCate Advanced Composites has done extensive research and found the properties for the woven semi-pregs. The data used in this research is taken from the datasheet provided by TenCate [22].

For thin walled woven fabrics, Kirchhoff's hypothesis for bending of thin plates is valid and hence classical laminate theory can be applied for the analysis. The principle directions for a single ply and for the entire laminate are shown in the fig 2-1 and 2-2.

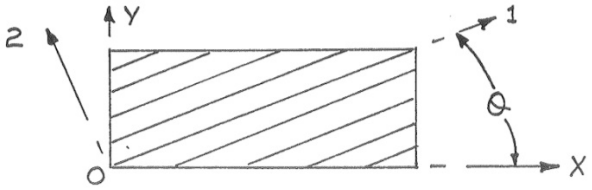

Fig 2-1 Coordinate systems for single ply

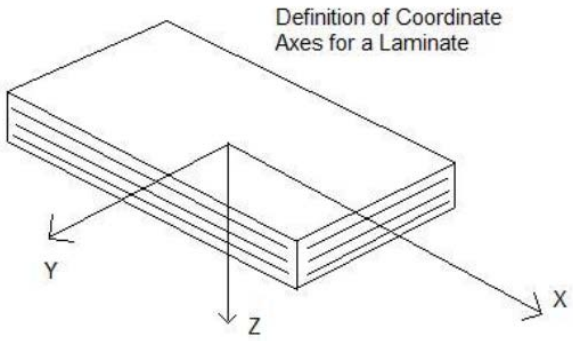

Fig 2-2 Global coordinate system applied to the laminate

Where 1, 2 represent the fiber directions (principle coordinate directions) and x, y and z represent the global directions for the entire laminate. According to the classical laminate theory, the transverse normal strain is negligible, there is no slip between individual

layers and each ply obeys the Hook's law. Applying the Hook's law in plane stress condition for an orthotropic material (each ply) in its principle coordinate directions, the compliance matrix that has no stress-strain coupling, can be written as follows

$$\begin{Bmatrix} \epsilon_1 \\ \epsilon_2 \\ \gamma_{12} \end{Bmatrix} = \begin{bmatrix} 1/E_1 & -\nu_{21}/E_2 & 0 \\ -\nu_{12}/E_1 & 1/E_2 & 0 \\ 0 & 0 & 1/G_{12} \end{bmatrix} \begin{Bmatrix} \sigma_1 \\ \sigma_2 \\ \tau_{12} \end{Bmatrix}$$

$$\{\epsilon\} = [S]*\{\sigma\}$$

Inverting the relation, in the 1-2 coordinate system, we get

$$\{\sigma\} = [Q] * \{\epsilon\}$$

The [Q] matrix can denoted as

$$\boldsymbol{Q}_{ij} = \begin{bmatrix} Q_{11} & Q_{12} & 0 \\ Q_{12} & Q_{22} & 0 \\ 0 & 0 & Q_{66} \end{bmatrix}$$

$$Q_{11} = \frac{E_{11}^2}{(E_{11} - \upsilon_{12} \cdot E_{22})}, \quad Q_{12} = \frac{\upsilon_{12} E_{11} E_{22}}{E_{11} - \upsilon_{12}^2 E_{22}}$$

$$Q_{22} = \frac{E_{11} E_{22}}{E_{11} - \upsilon_{12}^2 E_{22}}, \quad Q_{66} = G_{12}$$

Converting the material properties from principle directions to global coordinate systems using the transformation matrix.

$$\{\epsilon_{(x\text{-}y)}\} = \overline{Q_{ij}} * \{\sigma_{(x\text{-}y)}\}$$

The $\overline{Q_{ij}}$ can be expanded as

$$\begin{aligned}
\overline{Q_{11}} &= Q_{11}\cos(\theta)^4 + 2(Q_{12} + 2Q_{66})\cos(\theta)^2 \cdot \sin(\theta)^2 + Q_{22}\sin(\theta)^4 \\
\overline{Q_{12}} &= \overline{Q_{21}} = Q_{12}(\cos(\theta)^4 + \sin(\theta)^4) + (Q_{11} + Q_{22} - 4Q_{66})\cos(\theta)^2 \sin(\theta)^2 \\
\overline{Q_{16}} &= \overline{Q_{61}} = (Q_{11} - Q_{12} - 2Q_{66})\cos(\theta)^3 \sin(\theta) - (Q_{22} - Q_{12} - 2Q_{66})\cos(\theta)\sin(\theta)^3 \\
\overline{Q_{22}} &= Q_{11}\sin(\theta)^4 + 2(Q_{12} + 2Q_{66})\cos(\theta)^2 \sin(\theta)^2 + Q_{22}\cos(\theta)^4 \\
\overline{Q_{26}} &= \overline{Q_{62}} = (Q_{11} - Q_{12} - 2Q_{66})\cos(\theta)\sin(\theta)^3 - (Q_{22} - Q_{12} - 2Q_{66})\cos(\theta)^3 \sin(\theta) \\
\overline{Q_{66}} &= (Q_{11} + Q_{22} - 2Q_{12} - 2Q_{66})\cos(\theta)^2 \sin(\theta)^2 + Q_{66}(\cos(\theta)^4 + \sin(\theta)^4)
\end{aligned}$$

$$\overline{\boldsymbol{Q}_{ij}} = \begin{matrix} \overline{Q_{11}} & \overline{Q_{12}} & \overline{Q_{16}} \\ \overline{Q_{12}} & \overline{Q_{22}} & \overline{Q_{26}} \\ \overline{Q_{16}} & \overline{Q_{26}} & \overline{Q_{66}} \end{matrix}$$

For 'kth' ply, the stress components are given by

$$\begin{Bmatrix} \sigma_{xx} \\ \sigma_{yy} \\ \sigma_{xy} \end{Bmatrix}_k = \begin{bmatrix} \bar{Q}_{11} & \bar{Q}_{12} & \bar{Q}_{16} \\ \bar{Q}_{12} & \bar{Q}_{22} & \bar{Q}_{26} \\ \bar{Q}_{16} & \bar{Q}_{26} & \bar{Q}_{66} \end{bmatrix}_k \left[\begin{Bmatrix} \varepsilon_x^0 \\ \varepsilon_y^0 \\ \gamma_{xy}^0 \end{Bmatrix} + z \begin{Bmatrix} \kappa_x \\ \kappa_y \\ \kappa_{xy} \end{Bmatrix} \right]$$

Fig 2-3 Ply wise stresses in terms of material properties, strains and curvatures

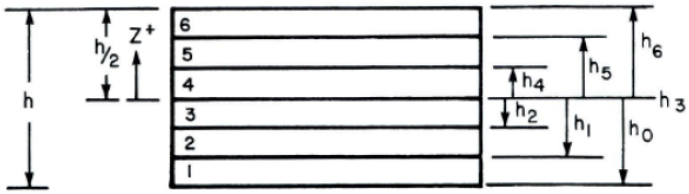

Fig 2-4 Laminate structure with ply numbers and distances

The plate resultant forces and moment within a laminate can be expressed as follows where 'h' is thickness of the laminate structure.

$$\mathbf{N} = \int_{-h/2}^{+h/2} \boldsymbol{\sigma}\, dz = \sum_{k=1}^{N} \int_{z_k}^{z_{k+1}} \boldsymbol{\sigma}_k\, dz \qquad \mathbf{M} = \int_{-h/2}^{+h/2} \boldsymbol{\sigma} z\, dz$$

$$\begin{Bmatrix} N_x \\ N_y \\ N_{xy} \end{Bmatrix} = \sum_{k=1}^{N} [\bar{Q}]_k \left(\int_{z_{k-1}}^{z_k} \begin{Bmatrix} \varepsilon_x^0 \\ \varepsilon_y^0 \\ \gamma_{xy}^0 \end{Bmatrix} dz + \int_{z_{k-1}}^{z_k} z \begin{Bmatrix} \kappa_x \\ \kappa_y \\ \kappa_{xy} \end{Bmatrix} dz \right)$$

$$\begin{Bmatrix} M_x \\ M_y \\ M_{xy} \end{Bmatrix} = \sum_{k=1}^{N} [\bar{Q}]_k \left(\int_{z_{k-1}}^{z_k} z \begin{Bmatrix} \varepsilon_x^0 \\ \varepsilon_y^0 \\ \gamma_{xy}^0 \end{Bmatrix} dz + \int_{z_{k-1}}^{z_k} z^2 \begin{Bmatrix} \kappa_x \\ \kappa_y \\ \kappa_{xy} \end{Bmatrix} dz \right)$$

The ε°_x, ε°_y and γ°_{xy} are the mid surface strains and κ_x, κ_y and κ_{xy} are the mid-surface curvatures. The mid-surface strains and curvatures are independent of 'z' and therefore the forces and moments can be written as

$$\begin{Bmatrix} N_x \\ N_y \\ N_{xy} \\ \hline M_x \\ M_y \\ M_{xy} \end{Bmatrix} = \left[\begin{array}{ccc|ccc} A_{11} & A_{12} & A_{16} & B_{11} & B_{12} & B_{16} \\ A_{12} & A_{22} & A_{26} & B_{12} & B_{22} & B_{26} \\ A_{16} & A_{26} & A_{66} & B_{16} & B_{26} & B_{66} \\ \hline B_{11} & B_{12} & B_{16} & D_{11} & D_{12} & D_{16} \\ B_{12} & B_{22} & B_{26} & D_{12} & D_{22} & D_{26} \\ B_{16} & B_{26} & B_{66} & D_{16} & D_{26} & D_{66} \end{array}\right] \begin{Bmatrix} \varepsilon_x^0 \\ \varepsilon_y^0 \\ \gamma_{xy}^0 \\ \hline \kappa_x \\ \kappa_y \\ \kappa_{xy} \end{Bmatrix}$$

Where [A], [B] and [D] can be defined as

$$[A_{ij}] = \sum_{k=1}^{N} [\bar{Q}_{ij}]_k (z_k - z_{k-1})$$

$$[B_{ij}] = \frac{1}{2} \sum_{k=1}^{N} [\bar{Q}_{ij}]_k (z_k^2 - z_{k-1}^2)$$

$$[D_{ij}] = \frac{1}{3} \sum_{k=1}^{N} [\bar{Q}_{ij}]_k (z_k^3 - z_{k-1}^3)$$

$[A_{ij}]$ is the extensional stiffness matrix, $[B_{ij}]$ is extension-bending coupling matrix and $[D_{ij}]$ is the bending stiffness matrix. As it can be seen, $[A_{ij}]$ is a function of $[Q_{ij}]$ which are the material properties and 't_k' which is the layer thickness. Hence the $[A_{ij}]$ matrix is not affected by the position of a particular ply in the laminate. $[B_{ij}]$ matrix usually becomes zero for a symmetric layup. The bending stiffness matrix $[D_{ij}]$ depends upon the $[Q_{ij}]$, thickness of the ply and position of the ply with respect to the mid-plane.

Thus it can be said that the flexural stiffness of a laminate is represented by the [D] matrix. The number of variables in the bending stiffness matrix can be reduced by

introducing invariants. Invariants were introduced by Tsai and Pagano [21] and can be written in terms of trigonometric identities as follows.

$\cos^4\theta = (1/8)*(3+ 4\cos2\theta + \cos4\theta)$ (1)

$\cos^3\theta\sin\theta = (1/8)*(2\sin2\theta + \sin4\theta)$ (2)

$\cos^2\theta\sin^2\theta = (1/8)*(1 - \cos4\theta)$ (3)

$\cos\theta\sin^3\theta = (1/8)*(2\sin2\theta - \sin4\theta)$ (4)

$\sin^4\theta = (1/8)*(3 - 4\cos2\theta + \cos4\theta)$ (5)

$U_1 = (1/8)*(3Q_{11} + 3Q_{22} + 2Q_{12} + 4Q_{66})$ (6)

$U_2 = (1/2)*(Q_{11} - Q_{22})$ (7)

$U_3 = (1/8)*(Q_{11} + Q_{22} - 2Q_{12} - 4Q_{66})$ (8)

$U_4 = (1/8)*(Q_{11} + Q_{22} + 6Q_{12} - 4Q_{66})$ (9)

$U_5 = (1/8)*(Q_{11} + Q_{22} - 2Q_{12} + 4Q_{66})$ (10)

The material properties can be written in terms of invariants as

$$\begin{Bmatrix} \overline{Q}_{11} \\ \overline{Q}_{22} \\ \overline{Q}_{12} \\ \overline{Q}_{66} \\ \overline{Q}_{16} \\ \overline{Q}_{26} \end{Bmatrix} = \begin{bmatrix} U_1 & \cos 2\theta & \cos 4\theta \\ U_1 & -\cos 2\theta & \cos 4\theta \\ U_4 & 0 & -\cos 4\theta \\ U_5 & 0 & -\cos 4\theta \\ 0 & \sin 2\theta/2 & \sin 4\theta \\ 0 & \sin 2\theta/2 & -\sin 4\theta \end{bmatrix} \begin{Bmatrix} 1 \\ U_2 \\ U_3 \end{Bmatrix}$$

Considering only the terms A_{11}, B_{11} and D_{11}

$$(A_{11}, B_{11}, D_{11}) = \int \overline{Q}_{11}(1, z, z^2)\, dz$$

$$(A_{11}, B_{11}, D_{11}) = \int [U_1(1, z, z^2) + U_2 \cos 2\theta(1, z, z^2) + U_3 \cos 4\theta(1, z, z^2)]\, dz$$

If every ply in a laminate is same, then the constants U1, U2 and U3 can be brought outside the integration and the terms can be written as

$$(A_{11}, B_{11}, D_{11}) = U_1\left(h, 0, \frac{h^3}{12}\right) + U_2\int_{-h/2}^{h/2}\cos 2\theta(1, z, z^2)\,dz + U_3\int_{-h/2}^{h/2}\cos 4\theta(1, z, z^2)\,dz$$

All the terms contain an integration combination of θ and z. The integration term can be written as follows

$$V_{0(A,B,D)} = \left(h, 0, \frac{h^3}{12}\right)$$

$$V_{1(A,B,D)} = \int \cos 2\theta(1, z, z^2)\,dz \quad V_{2(A,B,D)} = \int \sin 2\theta(1, z, z^2)\,dz$$

$$V_{3(A,B,D)} = \int \cos 4\theta(1, z, z^2)\,dz \quad V_{4(A,B,D)} = \int \sin 4\theta(1, z, z^2)\,dz$$

The [D] matrix for a laminate can be written in terms of these constants as

$$\{D\} = [U] * \{V\}$$

D_{11}		U1	U2	0	U3	0		V_{0D}
D_{22}		U1	-U2	0	U3	0		V_{1D}
D_{12}	=	U4	0	0	-U3	0	*	V_{2D}
D_{66}		U5	0	0	-U3	0		V_{3D}
D_{16}		0	0	-U2/2	0	-U3		V_{4D}
D_{26}		0	0	-U2/2	0	U3		

From the matrix it can be seen that if the laminate is made up single type of material, the maximum flexural stiffness is dependent on the angle of every ply and its position in the laminate. Based on this, different laminate configurations can be tried for maximum flexural stiffness.

Using the CLT the bending compliance and bending stiffness for a laminate layup with width ‘b’ can be calculated as

$$[d] = [D]^{-1}$$

The flexural modulus for the laminate can be written as

$$Ef = 12/(h^3 * d_{11})$$

2.2 Interlaminar Strength

The geometry of the ‘clips’ varies according to its function. However most of the clips have curvatures which are prone to bending and shear effects. The stress distribution through the thickness of the laminates changes with the material, geometry or load pattern. Delamination growth is the most common and biggest cause of failure in curved section of the laminates and is highly sensitive to the change in the core material in a laminate.

A lot of research has been done on determination of interlaminar or out-of-plane stresses within a laminate. The study of interlaminar strength becomes important as they are difficult to predict than in-plane stresses. Pipes and Pagano [22] have used the free-edge effect to do a detailed through the thickness stress analysis. They explained the influence of interlaminar stresses on the delamination and ultimately on the ultimate failure by using free edge effect. NASA [23] did early research on curved unidirectional graphite/epoxy composite laminates. The curved laminate was loaded till it failed at different depths through the thickness until virtually all the stiffness was lost. In the research, it was found that the delamination started at the center ply and rapidly grew into the legs of the specimen. During the delamination of center plies, value of stress in the surrounding layers also reach the point where the delaminations starts. This is how the delamination growth progresses through the laminate and the failure was observed through various layers along the thickness. The delamination initiation or the interlaminar

stresses can be theoretically predicted using the closed form elasticity solution. One way of determining the interlaminar stresses is by subjecting a curved beam to pure bending by applying end moments. This causes the laminate beam to open up and fail in delamination. Using this method the stress distribution can be found ply-wise and the effect of changing the core plies on the interlaminar strength can be investigated. Fu-Kuo Chang et al [24]used a similar method to calculate the stresses and strains through the loaded composite elbow (angle between the legs is 90°).

The closed form elasticity function can be developed based on anisotropic continuum theory. According to the anisotropic continuum theory, an Airy's stress function can be defined in cylindrical coordinate system for a beam with end moments. Jackson et al [25] defined the Airy's function for this problem as follows

$$F = [A' + B' r^2 + C' r^{(1+k)} + D' r^{(1-k)}]$$

Where A', B', C' and D' are arbitrary constants to be determined from the boundary conditions and k is a material constant which can be defined as

$$k = \sqrt{(\frac{E\theta}{E_r})} \tag{11}$$

For a beam under pure bending, the stress components do not vary with θ. Hence the equations of equilibrium for the plane stress reduce to

$$\frac{\partial \sigma_r}{\partial r} + \frac{\sigma_r - \sigma_\theta}{r} = 0 \qquad \frac{\partial \tau_{r\theta}}{\partial r} + 2\,\frac{\tau_{r\theta}}{r} = 0$$

The stresses in a cylindrically anisotropic body may be expressed in terms of stress function as

$$\sigma_r = \frac{1}{r}\frac{\partial F}{\partial r} + \frac{1}{r^2}\frac{\partial^2 F}{\partial \theta^2}$$
$$\sigma_\theta = -\frac{\partial^2 F}{\partial r^2}$$
$$\tau_{r\theta} = -\frac{\partial^2}{\partial r \partial \theta}\left(\frac{F}{r}\right)$$

Assuming plane stress conditions, the stress-strain relationship can be expressed as

$$\epsilon_r = \frac{1}{E_r}\sigma_r - \frac{\nu_{\theta r}}{E_\theta}\sigma_\theta$$
$$\epsilon_\theta = -\frac{\nu_{r\theta}}{E_r}\sigma_r + \frac{1}{E_\theta}\sigma_\theta$$
$$\gamma_{r\theta} = \frac{1}{G_{r\theta}}\tau_{r\theta}$$

And the strain-displacement relationship can be written as

$$\epsilon_r = \frac{\partial u_r}{\partial r}$$
$$\epsilon_\theta = \frac{1}{r}\frac{\partial u_\theta}{\partial \theta} + \frac{u_r}{r}$$
$$\gamma_{r\theta} = \frac{1}{2}\left(\frac{1}{r}\frac{\partial u_r}{\partial \theta} + \frac{\partial u_\theta}{\partial r} - \frac{u_\theta}{r}\right)$$

Using the Airy function, the stresses on application of end moments can be written as:

$$\sigma_r(r) = 2B' + C'(1+k)r^{k-1} + D'(1-k)r^{-k-1}$$
$$\sigma_\theta(r) = 2B' + C'k(1+k)r^{k-1} - D'k(1-k)r^{-k-1}$$
$$\tau_{r\theta} = 0$$

Substituting the value of stresses, the displacements for the end moments can be written as

$$u_r(r) = B'\left\{2r\left(\frac{1}{E_r} - \frac{\nu_{\theta r}}{E_\theta}\right)\right\} + C'\left\{(1+k)r^k\left(\frac{1}{k}\frac{1}{E_r} - \frac{\nu_{\theta r}}{E_\theta}\right)\right\} - D'\left\{(1-k)r^{-k}\left(\frac{1}{k}\frac{1}{E_r} + \frac{\nu_{\theta r}}{E_\theta}\right)\right\}$$
$$u_\theta(r,\theta) = B'\left\{2r\left(\frac{1}{E_\theta} - \frac{1}{E_r}\right)\right\}\theta$$

For a single layer curved beam, the unknowns can be determined from the boundary conditions to give a closed form solution for the stresses and the displacement. In a laminated beam comprising of 'N' layers of plies, the boundary conditions can be written for multiple layers as

At surfaces between the layers, where $r=a_i$

$$\sigma_r^{(i)}(a_i) = \sigma_r^{(i+1)}(a_i)$$
$$u_r^{(i)}(a_i) = u_r^{(i+1)}(a_i)$$
$$u_\theta^{(i)}(a_i) = u_\theta^{(i+1)}(a_i)$$

At the inner radius of curvature $r=a_0$

$$\sigma_r^{(1)}(a) = 0$$

At the outer radius of curvature $r=a_n=b$

$$\sigma_r^{(N)}(b) = 0$$

For loading conditions, the above boundary conditions gives 3N-1 equations with 3N constants. The last equation needed is the loading equation. The total end moment applied on the curved bar can be written as

$$-M = \sum_{i=1}^{N} \int_{a_{i-1}}^{a_i} (r - r_0)\sigma_\theta(r)\,dr$$

For pure bending, the r_0 term vanishes and the resultant moment can be written as

$$-M = \sum_{i=1}^{N} \int_{a_{i-1}}^{a_i} r\sigma_\theta(r)\,dr$$

Hence by solving these equation with finite element method, the stresses and displacements in each ply can be found for a beam under pure bending.

Considering the entire beam, Lekhnitskii presented the equations for cylindrically anisotropic curved beam under pure bending. The stresses in the radial direction and tangential direction experienced by the entire laminate are given as

$$\sigma_{\mathrm{r}} = -\frac{M}{{R_{\mathrm{o}}}^2 bg}\left[1 - \frac{1-c^{k+1}}{1-c^{2k}}\left(\frac{r}{R_{\mathrm{o}}}\right)^{k-1} - \frac{1-c^{k-1}}{1-c^{2k}}\, c^{k+1}\left(\frac{R_{\mathrm{o}}}{r}\right)^{k+1}\right]$$

$$\sigma\theta = -\frac{M}{{R_{\mathrm{o}}}^2 bg}\left[1 - \frac{1-c^{k+1}}{1-c^{2k}}\, k\left(\frac{r}{R_{\mathrm{o}}}\right)^{k-1} + \frac{1-c^{k-1}}{1-c^{2k}}\, k\, c^{k+1}\left(\frac{R_{\mathrm{o}}}{r}\right)^{k+1}\right]$$

$$\tau_{\mathrm{r}}\theta = 0$$

Where $r = \left(\frac{(k+1)\left(1-c^{k-1}\right)c(R_{\mathrm{i}}R_{\mathrm{o}})^{k}}{(k-1)\left(1-c^{k+1}\right)}\right)^{\frac{1}{2k}}$,

$c = R_{\mathrm{i}}/R_{\mathrm{o}} \qquad g = \frac{1-c^2}{2} - \left(\frac{k}{k+1}\right)\left(\frac{\left(1-c^{k+1}\right)^2}{1-c^{2k}}\right) + \left(\frac{kc^2}{k-1}\right)\left(\frac{\left(1-c^{k-1}\right)^2}{1-c^{2k}}\right)$

This research tries to understand the failure progression through curved hybrid thermoplastic laminates subjected to pure bending.

2.3 Bearing strength

The ‘clips’ are generally used to connect the fuselage shells to the interior composite rib structures. Usually this connection is mechanical, done by bolts or rivets which necessitates holes being drilled in the ‘clip’ structure. The major modes of failure for a composite bolted joint are net tension, shear out or bearing failure. Tension failure occur at the minimum cross section area mostly along a line where the stress concentration is maximum. In tension failure, the failure initiates at the hole edge and propagates in the direction normal to that of the applied load. Failure of the joint in shear is called as shear pullout. This is a result of shear failure in two parallel planes which are tangential to the

hole edge and extend to the free edge in the direction parallel to the applied load. Bearing failure is defined as local compressive failure in the material immediately under the loaded bolt. Out of the three failure phenomenon associated with bolt failures, tension and shear failure causes catastrophic failures of the entire clip structure.

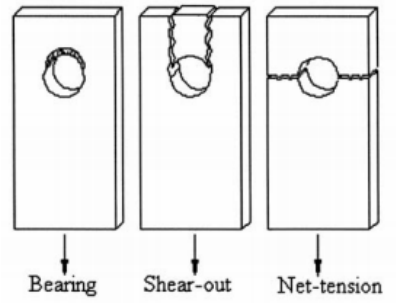

Fig 2-5 Different modes of failure for a bolted sample

The mode of failure in a laminate joint depends upon various factors like edge distance, width, depth, stacking sequence and ply orientation. According to Hart [26], net tension generally occurs in a specimen with lower width to diameter ratio or with lower edge distance to diameter ratio. When the edge distance between the loaded bolt and edge of a composite laminate is small or the layup pattern is deficient in ±45° plies, the predominant mode of failure is shear out or cleavage. The failure modes changes from tension to bearing as the width/depth ratio increases whereas as edge distance/depth ratio decreases, the failure mode changes from bearing to shear [27].

Out of the three modes of failure in bolted joints, bearing failure in the laminates was studied in this research. Bearing failure can be described as localized compression failure in area under the bolt. The mechanism of bearing failure is complex and depends on many parameters such as lateral constraint, ply orientation, stacking sequence and

clamping force. Collings [27] reported that out of the three failure modes, bearing strength is most sensitive to the stacking sequence. Park [28] and Chang [24] studied the influence of stacking sequence and clamping force experimentally on the ultimate bearing strength of bolted joints. Park used the acoustic emission technique to identify the onset of delamination in the laminate. It was found that placing 0° plies near the center of the laminate increases the ultimate bearing strength as compared to placing 90° plies. Also the bearing strength increased with increase in clamping torque. Higher the clamping torque, higher the delamination is suppressed and the damage changes from catastrophic to progressive one.

The bearing failure starts with local compressive damage in the contact region between the bolt and hole surface and the damage progresses further depending on the material stiffness. The presence of bolt and washer arrests the out-of-plane damage and the compression failure progresses in-plane. There are various phenomenon associated with bearing failure like microbuckling, fiber crushing, fiber kinking and transverse matrix cracks. Microbuckling is defined as localized buckling of fibers under load. It often leads to fiber crushing as the load increases [29]. Fiber kinking can be defined as shear deformation of a band of fibers within the matrix. The fibers are usually broken at the edge of the shear band. Microbuckling and fiber kinking are various localized compressive failure modes experienced by the contact region during loading.

According to Xiao et al [32], the local compressive damage causes fiber kinking in the areas surrounding the hole followed by matrix cracking. The fiber kinking induces shear

cracks in 45 plies and causes delamination. As the load on the laminate grows, the cracks spread through the thickness and cause failures. Sun [30] developed a fiber microbuckling model and found that the percentage of 0° plies play an important role in damage initiation. Also they observed transverse matrix cracking in the laminate before the microbuckling. Thus it can be seen that the bearing failure is a complex phenomenon which consists of combination of different phenomena like fiber microbuckling, fiber kinking, matrix cracks.

Over the years lots of attempt have been done to predict the bearing strength and to model all the associated phenomena and parameters. One way to predict the bearing failure was by calculating the ‘characteristic length’. Camanho and Lambert [31] used the average stress model and point stress model to calculate the characteristic distances and uses the LaRC04 failure criteria to predict ultimate failure stresses in each ply. The other way was to simulate the bearing failure using finite element methods for different boundary conditions. Camanho et al [32] gave a three dimensional finite element model to predict the response of a mechanically fastened joints in unidirectional composite laminate loaded in tension, shear or bearing and validated the results using experimentation. The model is able to predict the damage initiation and its progress through the laminate. For woven thermoplastic laminates, Vieille et al [33] conducted experimental research on bearing failure. He documented that as the load increases, the damage begins at the contact area between the bolt and the laminate and then progresses through the phenomena of micro-buckling and transverse matrix cracks.

For hybrids the failure depends on compressive behavior of both the fiber systems. According to Matthews et al [34], the bearing strength of a composite depends upon the fiber volume fraction of carbon fiber within the laminate. Higher is the carbon fiber ratio, closer is the bearing strength of the hybrid to that of all carbon laminate. Also the mode of failure changes from brittle as in case with all carbon to ductile with addition of glass fibers in the laminate. However there hasn't been much experimental research done in the area of bearing response of thermoplastic hybrids. This research sheds some light on the behavior of hybrid carbon-PPS laminates during bearing failure in bolted joints.

CHAPTER 3. MATERIALS

From the literature review it was established that the flexural response of a laminate depends upon the stacking sequence of the individual plies and the distance of the plies from the mid-plane. Keeping this in mind, the inter-ply hybrids in this research were created by replacing the carbon layers near the mid-plane with other materials. The materials which are to be used in the laminates are limited by the processibility, availability, handling, weight and cost.

The original laminates are made using woven carbon-PPS. The material was provided by TenCate Advanced Composites, Netherlands and was five harness satin weave carbon fabric powder coated with PPS resin having 50% fiber volume fraction. The material to be placed near the mid-plane in the laminate should be able to take the high processing temperatures and pressures used with the carbon-PPS laminates. Also it should not increase the weight of the laminate too much as compared to the original laminate. Some of the options which fit the criteria were honeycomb structures like aluminium honeycomb, fiberglass phenolic honeycombs, high temperature foams, glass-PPS semi-preg and random discontinuous long fiber carbon-PPS flakes.

3.1 Honeycomb Structures

The honeycombs are light and easier to handle but they cannot be compression molded with the carbon-PPS as outer skins. They needed to be consolidated separately and attached using adhesives. This introduces a weal layer in the laminate. For honeycombs that can withstand the pressure, problem is that during the compression molding, the viscosity of PPS reduces which causes it to flow through the layers of the laminates. If the honeycomb structures are used as it is, the resin will pool into the honeycomb structure and causes poor consolidation of surface layers. This problem can be partially solved by filling the honeycomb structure using powdered PPS. However this method increases the weight of the laminates exponentially.

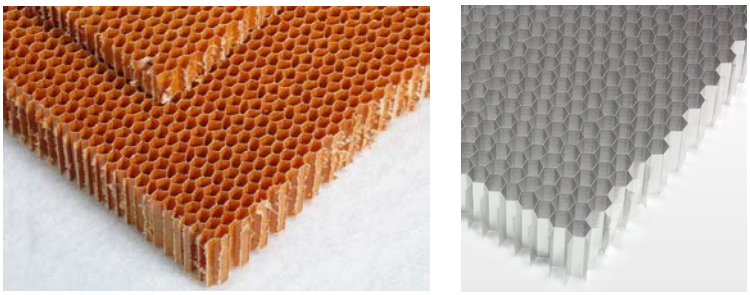

Fig 3-1 Phenolic and Aluminium honeycomb structures

3.2 Foams

Using foam between the carbon-PPS sheets was another option. Several companies like Du Pont produces high temperature and high pressure resistant foams. However these foams are expensive and require special handling.

Fig 3-2 High Temperature foams

3.3 Glass and Discontinuous CARBON-PPS FLAKES

Glass-PPS semi-preg and discontinuous long fiber carbon-PPS flakes proved to be most effective materials to combine with carbon-PPS pre-preg sheets to make hybrids. The materials require same temperature and process conditions as carbon-PPS thus eliminating any need for additional steps in manufacturing the laminates. Two different types of glass fabric were used along with random discontinuous long fiber carbon-PPS flakes. One type was twill weave glass fabric and other was 8 harness satin weave glass semi-preg powder coated with PPS resin. The material specifications and mechanical properties of the materials used in various calculations are given in the table below. In the material specification 127 denotes the length of the material roll in centimeters. The resin content by weight in semi-preg is 43% in carbon-PPS and 34% in glass-PPS.

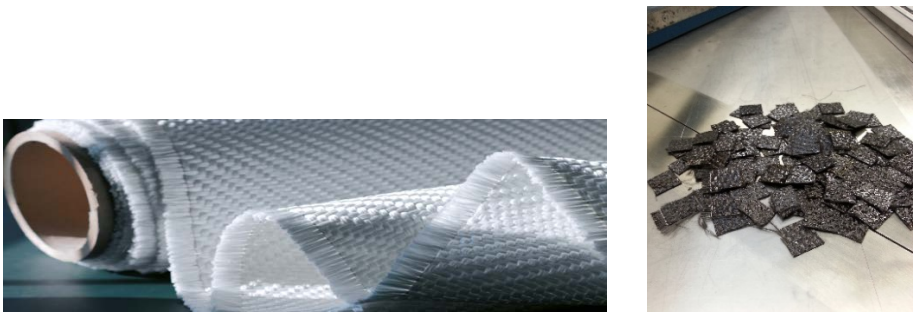

Fig 3-3 Glass fabric and discontinuous CARBON-PPS FLAKES

Table 3-1 Specification for material used in the research

Batch no	Material Specification	Material and Fabric style	Sizing compatibility	Thickness (mm)
10718292	2013-T-2-WRT0600- 2/2 V4	Glass fabric 2*2 twill weave	Polyamide	17
20140702	GF 7781 127 34%	Glass-PPS semi-preg 8 Harness satin weave	Polyphenlyene sulfide	9
20121787.03	CF 0286 127 43%	Carbon-PPS semi-preg 5 Harness satin weave	Polyphenylene sulfide	7

CHAPTER 4. MANUFACTURE OF LAMINATES

4.1 Flat laminates

The laminates of size 480mm*480mm were made with quasi-isotropic layup. The layup chosen for all the laminates was $[(0,90)/(45,-45)/(-45,45)/(0,90)]_s$ with 8 plies. The plies were laid and placed between two steel plates covered with Upilex release film. A thermocouple was placed between the plies to measure the internal temperature of the laminate during the hot press cycle. For a general ply layup the cross section of the laminate looks like fig 4-1. In different hybrids, the 4 and 5 no carbon plies, which are the nearest to the mid plane, were replaced with glass and discontinuous long fiber carbon-PPS flakes.

1 (0,90)
2 (45,-45)
3 (-45,45)
4 (0,90)
5 (0,90)
6 (-45,45)
7 (45,-45)
8 (0,90)

Fig 4-1 Laminate layup and ply numbers

The detail description of layup for the three hybrids is as follows:

Hybrid 1

Hybrid 1 was made by replacing two carbon layers (ply 4 and ply 5) with a single glass ply.

The glass ply used was GlassWRT0600 has higher filament diameter (17µm) than the carbon-PPS ply (7µm). Hence the glass ply is thicker than carbon-ply and therefore a single ply of glass was used instead of two carbon plies to maintain the overall thickness of the laminate. The glass fabric is twill weave which maintained the symmetry of the laminate even with odd number of plies. The resin content of the laminate was balanced at 50% by placing extra resin sheets within the laminate.

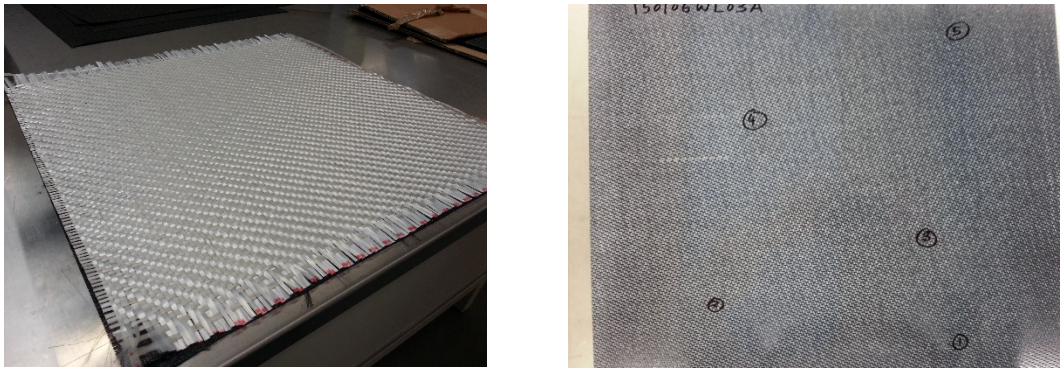

Fig 4-2 Hybrid 2 during layup and final consolidated laminate

Hybrid 2

Hybrid 2 was made by replacing two carbon layers (ply 4 and ply 5) with two glass-PPS plies. The glass-PPS plies were placed with orientation of (0,90). The glass fabric used is eight harness satin weave US7781 impregnated with PPS resin. The fabric is thinner than the original carbon-PPS ply and hence a decrease in the overall thickness of laminate is expected.

Hybrid 3

Hybrid 3 was made by replacing the two carbon layers by a thick layer of random discontinuous long fiber carbon-PPS flakes. Long fiber reinforced thermoplastic flakes typically have fiber length of 6mm and higher. As the fiber length increases, there will be

greater adhesion between the matrix and fibers and more effectively the stress can be transferred to the fibers. For the fiber length of 10mm-12mm the fiber pellets attain properties almost equal to continuous fiber thermoplastic. In this project, a thick layer of flakes of size 12mm*12mm are used to replace the two continuous carbon plies (ply 4 and ply 5). The carbon-PPS plies are manually cut into the flake size of 15mm*15mm at TenCate Advanced Composites but this process can be automated for larger production of the laminate

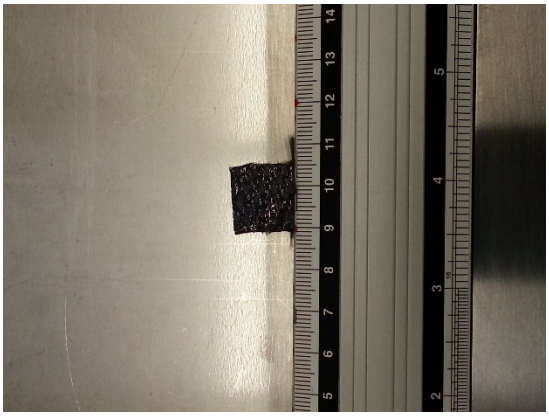

Fig 4-3 Discontinuous carbon-PPS flake

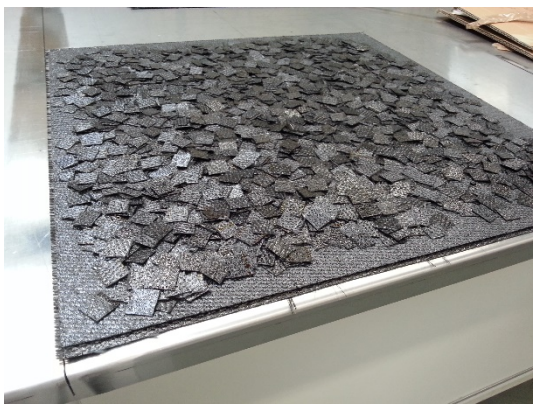

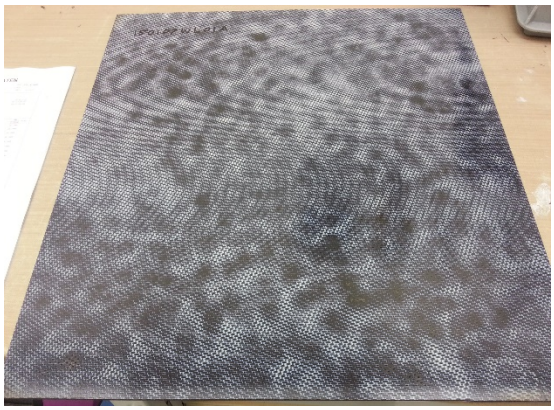

Fig 4-4 Hybrid 3 during layup and fully consolidated laminate

4.2 Press Cycle for flat laminates

The laminates are made by the process of compression molding. The process of compression molding consists of placing the layup in a preheated press and closing the mold with application of pressure. Throughout the entire process, heat and pressure are maintained on the part. For the semi-crystalline thermoplastic polymers like polyphenylene sulfide, the glass transition temperature is 90°C and the melting temperature is 285°C [38]. However at 285°C PPS still has some crystals and the polymer doesn't have appropriate viscosity to get good wettability. From the past literature [38] it was found that at 340°C, all the residual crystals in the polyphenylene sulfide melt. However exposure to temperatures higher than 320°C, the resin viscosity rises exponentially so that the processing becomes difficult. Also exposure to temperatures higher than melting temperature causes chain extension, degradation and cross linking in the presence of oxygen. This limits the processing time and temperature for the carbon-PPS semi-preg plies. For the laminates made in this research, a temperature of 310°C was selected which is found to give higher crystallinity in the consolidated laminates. The laminates are heated under a constant pressure of 10 bars for a time period of 20 mins and then cooled naturally under pressure till the temperature drops below 70°C or till it becomes easy to handle the laminate. The laminate was pressed in the hot press at TenCate Advanced Composites, Netherlands.

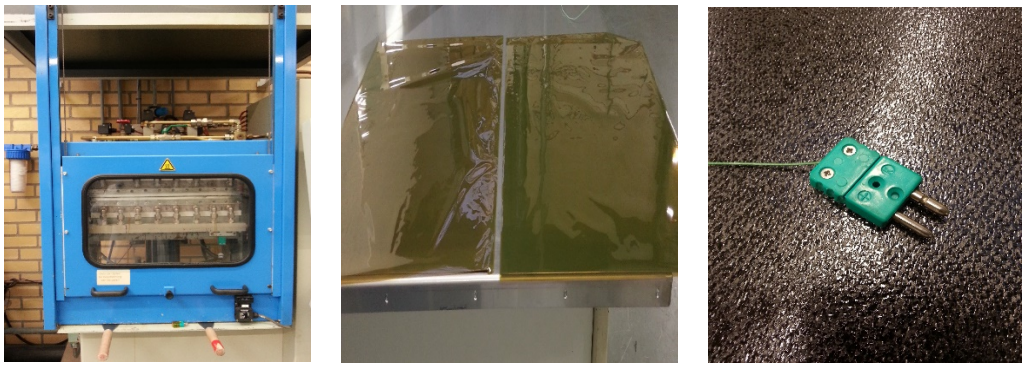

Fig 4-5 Hot press at TenCate with Upilex release films and thermocouple

Thermocouples in heated platens were mounted to measure the temperature of the steel plates, at the mid-plane of the laminate and temperature of the hot press.

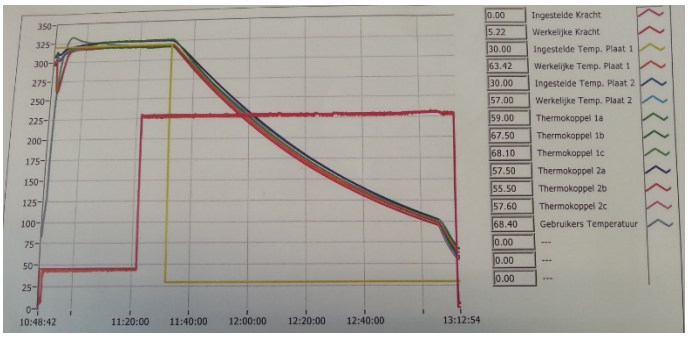

Fig 4-6 Temperature profile in the hot press

4.3 C-scans

The quality of laminate depends upon how well the laminate has been consolidated i.e what is the void content in the laminate. One way of determining this is by doing microscopy. However microscopy depends upon the sample location in the laminate and may not give a correct picture of the quality of entire laminate. The other way of finding the quality of laminate is performing an ultrasonic C-scan of the entire laminate.

The ultrasonic inspection works on pulse-echo method. For this research, the C-Scan was performed using RapidScan2 automated with a 5MHz 64 elt Lineair transducer and scanning velocity of 2795m/s. The scan maps the variation in the thickness in color throughout the laminate and any thicknesses below a certain threshold are picked up as voids. The variation in thickness is represented by a color scale with blue being minimum thickness and red being the highest thickness.

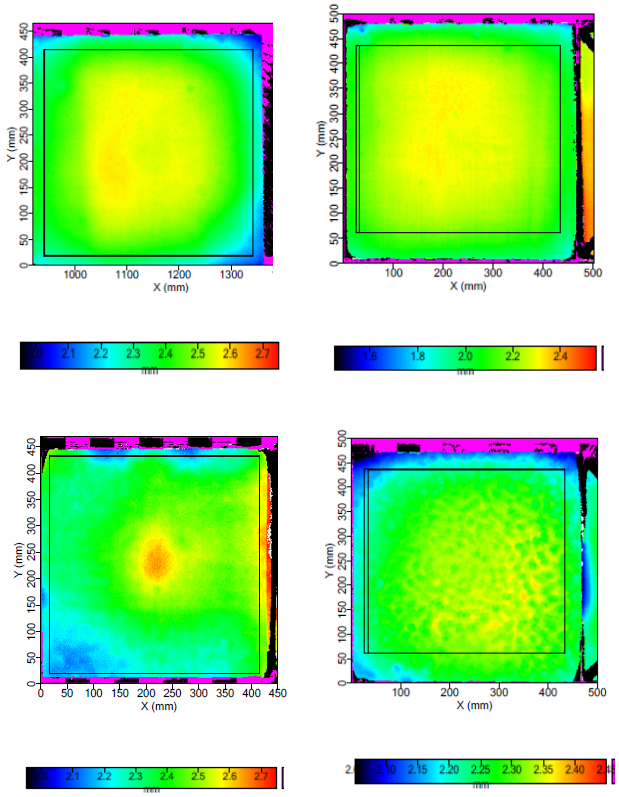

Fig 4-7 C-scans of different laminates

The C-scans show well consolidated laminates and no voids were detected. The variation of thickness is a result of resin flow during the consolidation. From the C-scans it was seen that most of the resin is spread in the central area of the laminate leading to higher thickness. The all-carbon-PPS and hybrid 1 showed low variation in the thickness.

Hybrid 2 showed a central region of higher thickness, possibly due to the accumulation of resin in that area mostly leading to low fiber volume fraction in that area. For the hybrid 3, with flakes, the c-scan detected the distribution of flakes throughout the laminate. This helps in relating the influence of distribution of flakes on the mechanical properties of the laminate. Based on the C-scans samples were taken from various positions in the laminate and fiber volume fraction was calculated by weighing the sample and by finding the volume to give an average value for the entire laminate.

Table 4-1 Volume fractions of the different constituents in laminates

Sample	Thickness (average) (mm)	Carbon (vol%)	Glass (vol%)
Carbon-PPS	2.54	50.56	0
Hybrid 1	2.24	43.28	11.05
Hybrid 2	2.33	42.72	10.91
Hybrid 3	2.34	54.91	0
Glass-PPS	2.03	0	59.80

4.4 V-shape laminates

Through the thickness strength of the laminates becomes a critical parameter for curved geometries such as bends and elbows. Hence it was important to test the behavior of curved joints under moments to gauge the response of the hybrids under loading. The v-shape samples were made using the method of thermoforming. Thermoforming involves reheating the consolidated laminates and pressing them into desired shape. There are different thermoforming methods such as match-die forming, rubber pad forming,

hydroforming, diaphragm forming, vacuum forming and autoclave forming. Match-die press forming is the mostly widely used technique presently [36] and was used to make the V-shape part for this project. Thermoforming was done at thermoplastic composite research center (TPRC) at Enschede, Netherlands.

4.5 Press Cycle for Thermoforming

Thermoforming consists of three steps, first step is heating the pre-consolidated laminates, second is part forming and reconsolidation in a matched tool and third part ejection coupled with part cooling. The pre-consolidated blanks are heated to a temperature above the melt temperature of PPS resin which causes redistribution of resin and help in reducing the void content in the laminate. The laminates were heated using the infrared oven upto a temperature of 320°C.

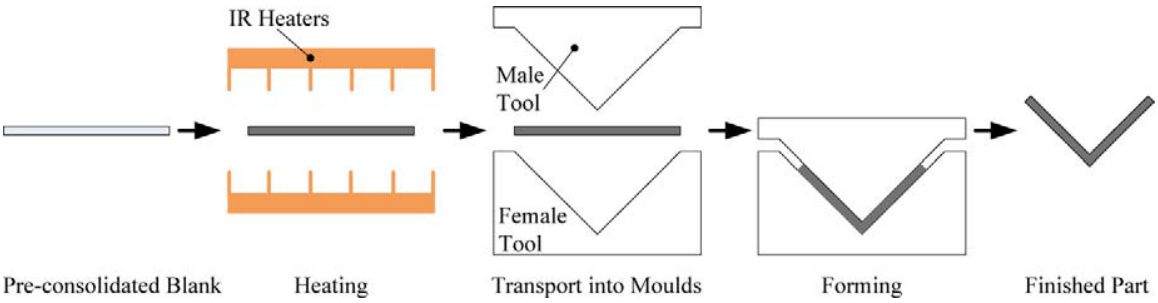

Fig 4-8 Schematic of the thermoforming process flow [37]

The heated laminate was then transferred into the mold. The molds were heated and held at a constant temperature of 200°C. The tool temperature was kept below the crystallization temperature of the PPS resin to avoid melting of the crystals. If the crystals melt and the resin is rapidly cooled, it may lead to the formation of amorphous structure within the laminate which may reduce the strength of the laminate [37]. The heated

laminate was then re-consolidated in the matched dies and ejected to be cooled naturally. The entire process from heated in infrared oven upto ejection took 170 secs. The final part is shown in the fig 4-10.

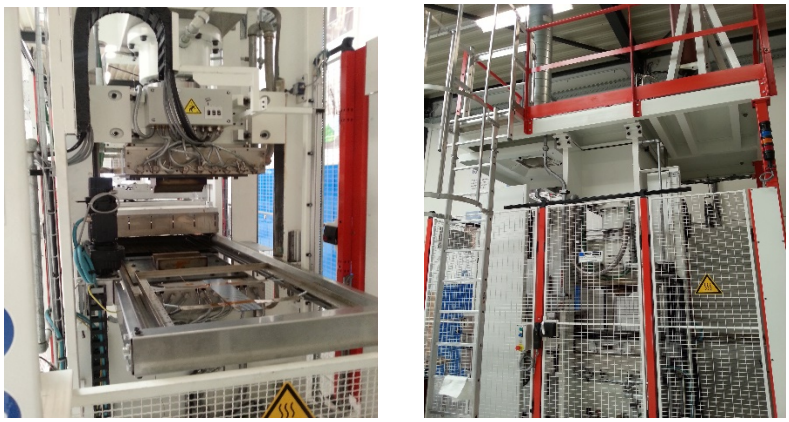

Fig 4-9 Thermoforming facility at TPRC, Netherlands

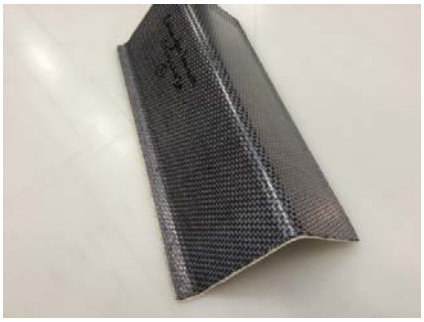

Fig 4-10 Laminate after thermoforming

Fig 4-11 Samples made after cutting using diamond saw

After the laminate cools to room temperature, individual specimens were cut for testing using a water cooled diamond saw. Since the laminate is heated above the melting point of the resin, the resin distribution throughout the laminate changes, thus changing the thickness of the curved laminate and fiber volume fraction from the flat laminates. The thickness of the curved specimens was measured at the curvature and at the legs and fiber volume fraction was calculated again using the areal weight of the plies. From the volume fractions higher resin content was observed in the curvature of v-shape sample as compared to its legs. This was attributed to fixed die thickness for all samples.

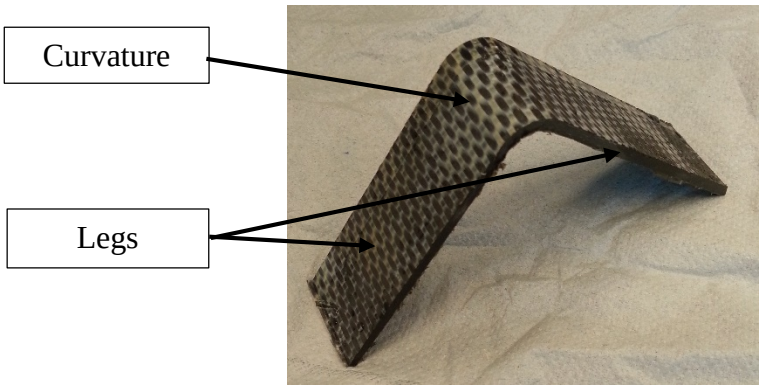

Fig 4-12 Test sample

Table 4-2 Volume fractions in legs and curvature of the sample

Sample	Carbon (vol%) (curvature)	Glass (vol%) (curvature)	Carbon (vol%) (legs)	Glass (vol%) (legs)
Carbon-PPS	36.02	0	50.94	0
Hybrid 1	25.96	6.53	40.66	10.38
Hybrid 2	27.02	6.89	48.0	12.25
Hybrid 3	34.89	0	48.38	0
Glass-PPS	0	25.58	0	62.70

A matched die set having a fixed thickness of 2.3mm was used. For samples having thickness greater than this, the pressure on the legs was greater than that on the curvature. Hence the resin pooled in the curvature giving resin rich area and lower fiber volume fraction.

CHAPTER 5. TESTING

5.1 Three point bend test

The flexural response of laminates was evaluated experimentally using the three point bend test. The test was carried according to the European standard EN2562 [39]. The test machine was Zwick020 and the test was carried out in a testing facility at TenCate Advanced Composites. The samples were cut into specified dimensions of 100mm (length) *10mm (width) using a water cooled diamond saw. Six samples were tested for every type of hybrid and all carbon-PPS and all glass-PPS laminates. The load is applied on the samples at the rate of 5mm/min. The test setup measures the force and the displacement of the sample and calculates the flexural strength and modulus based on these values.

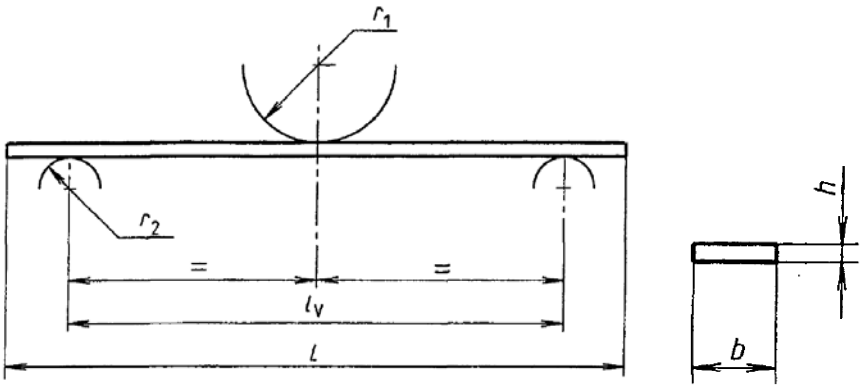

Fig 5-1 Free body diagram for the setup and sample in three point bending

The sample and setup dimensions have been given in the table.

Table 5-1 Sample and setup dimensions at TenCate Advanced Composites testing facility

Length (mm)	Span length L_v (mm)	Width b (mm)	r_1 (mm)	r_2 (mm)
100	80	10	12.5	5

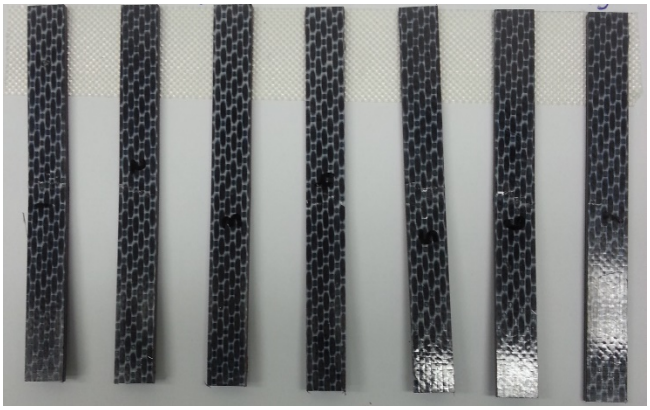

Fig 5-2 Test samples for carbon-PPS laminate

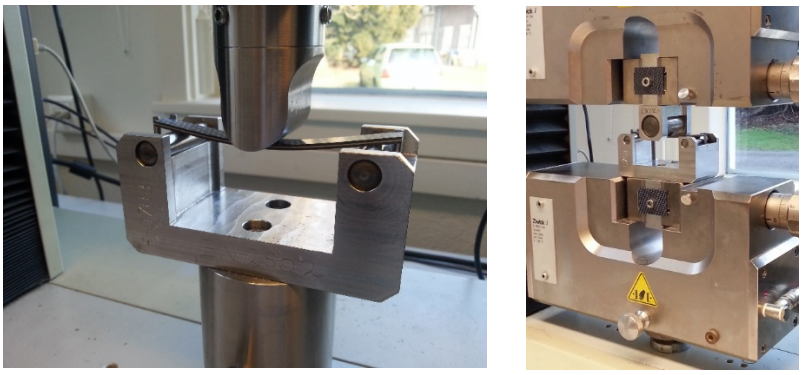

Fig 5-3 Test facility at TenCate Advanced Composites

According to the standard [39], flexural strength is defined as the maximum stress at outer surface of a flexure test sample corresponding to the peak applied force prior to the flexural failure. The flexural modulus is defined as the ratio of stress range to corresponding strain range of 0.1 to 0.5 of maximum force for a sample.

$$\sigma b = \frac{3\,P\,L_v}{2\,b\,h^2}$$

$$Ef = \frac{P\,{L_v}^3}{10\,b\,h^3(f_2 - f_1)}$$

Where σb = Flexural strength (MPa)

P = load at failure (N)

Ef = flexural modulus (GPa)

f2 = deflection corresponding to (P/10) load

f1 = deflection corresponding to (P/2) load

5.2 Four Point bend test for a curved beam

The four point bend test for curved beam was performed to evaluate the inter-laminar performance of the hybrids. The curved beam geometry was loaded with help of pure moments to induce fracture in curved section. This test was performed in accordance with ASTM D 6415 standard at testing facility at University of Twente. Six samples were tested for each type of hybrid along with all carbon-PPS and all glass-PPS laminates. The test was performed on the test setup 1445.

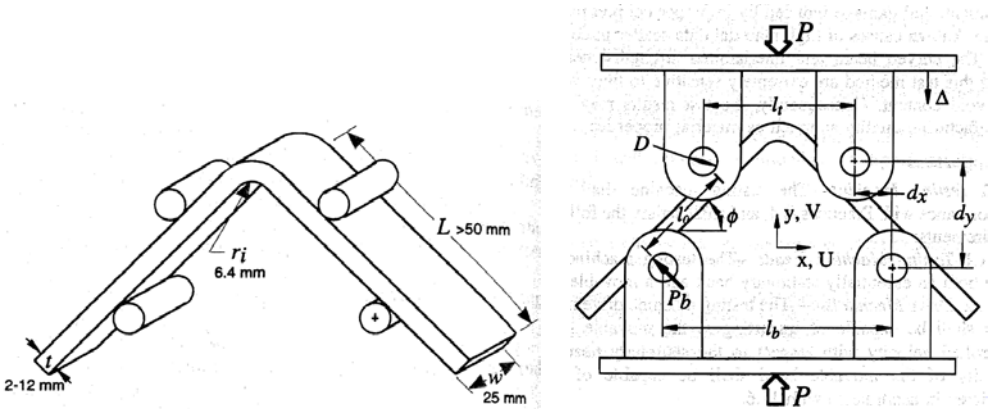

Fig 5-4 Free body diagram of test sample and test setup

The different measuremens needed for the test are as follows:

P : Load applied on the fixture (N)

l_t and l_b : distance between the centerlines of top and bottom loading bars (mm)

Δ : relative displacement between top and bottom fixtures (mm)

d_x : horizontal distance between two adjacent top and bottom loading bars (mm)

$d_x = (l_b - l_t)/2$

d_y : vertical distance between two adjacent top and bottom loading bars (mm)

D : diameter of cylindrical loading bars (mm)

P_b : force aplied to the sample by a single loading bar (N)

l_o : distance along sample legs between centerlines of top and bottom loading bar (mm)

ϕ : angle of legs of the sample with respect to horizontal

ϕ_i : angle of legs of the sample with respect to horizontal at the start

$$d_y = d_x \tan(\phi_i) + \frac{D + t}{\cos(\phi_i)} - \Delta$$

$$\phi = \sin^{-1}\left(\frac{-d_x (D + t) + d_y \sqrt{d_x^2 + d_y^2 - D^2 - 2Dt}}{d_x^2 + d_y^2}\right)$$

The test setup dimensions for the test are given in the table:

Table 5-2 Test setup dimensions

D (mm)	l_b (mm)	l_t (mm)	d_x (mm)
8	76.4	53.8	11.3

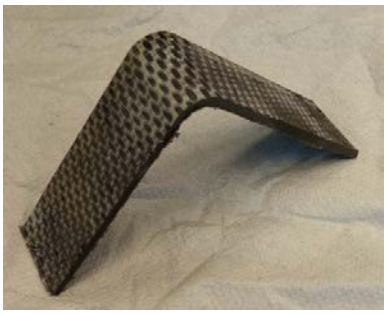

Fig 5-5 Test sample for four point bend test

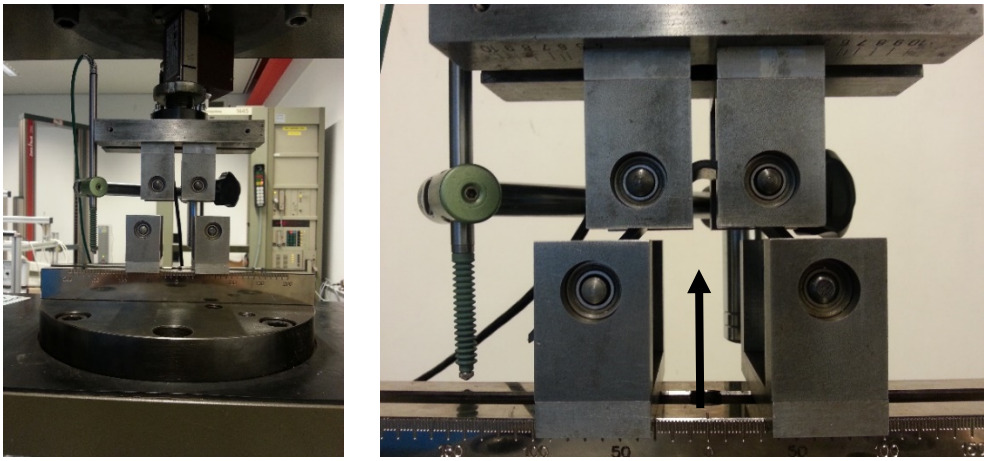

Fig 5-6 Test setup and LVDT at University of Twente

As shown in the fig, the lower fixture moves upwards at a rate of 5 mm/min causing the legs of the sample to open up. The vertical displacement of the lower fixture once the sample is loaded was measured by a linear variable differential transformer (LVDT).

The inner radius of the sample was in tension and the outer radius was in compression. The test was concluded as soon as the first failure occurs in a sample. The test calculates the curved beam strength and interlaminar tensile strength with the following formulae

$$CBS = \frac{M}{w} = \frac{P_b l_0}{w} = \left(\frac{P}{2w\cos(\phi)}\right)\left(\frac{d_x}{\cos(\phi)} + (D + t)\tan(\phi)\right)$$

$$\sigma_r = -\frac{CBS}{r_o^2 g}\left[1 - \frac{1-\rho^{\kappa+1}}{1-\rho^{2\kappa}}\left(\frac{r_m}{r_o}\right)^{\kappa-1} - \frac{1-\rho^{\kappa-1}}{1-\rho^{2\kappa}}\rho^{\kappa+1}\left(\frac{r_o}{r_m}\right)^{\kappa+1}\right]$$

$$g = \frac{1-\rho^2}{2} - \frac{\kappa}{\kappa+1}\,\frac{(1-\rho^{\kappa+1})}{1-\rho^{2\kappa}} + \frac{\kappa\rho^2}{\kappa-1}\,\frac{(1-\rho^{\kappa-1})^2}{1-\rho^{2\kappa}},\ \kappa = \sqrt{\frac{E_\theta}{E_r}},\ \rho = \frac{r_i}{r_o}$$

$$r_m = \left[\frac{(1-\rho^{\kappa-1})(\kappa+1)(\rho r_o)^{\kappa+1}}{(1-\rho^{\kappa+1})(\kappa-1)r_o^{-(\kappa-1)}}\right]^{\frac{1}{2\kappa}}$$

where g, ρ and κ are geometric and material constants.

5.3 Double Lap Shear test

The bearing response of the laminates was evaulated using double lap shear test. The test was carried out according to the Airbus standards AITM1-0009 on the test setup Zwick 1474 at TenCate Advanced Composites testing facility. The test setup is shown in the fig. The sample was clamped between the loading plates by a bolt and a torque of 1.3 Nm was applied to simulate ‘finger tight’ condition.

The load was applied by the machine clamps which pull the sample downwards against the bolt at a crosshead rate of 1 mm/min. The test was stopped after a load drop of 50% or 20% hole deformation, whichever occurs first. The hole deformation was recorded using a clip-on extensometer mounted on the sample. The extensometer measures the change in length between its prongs during the experiment. Since the extensometer was so mounted that one of its prongs rests on the edge of the hole, any elongation in the hole diameter gets recorded as change in length of extensometer. Five samples of each hybrid and all-carbon-PPS and all-glass-PPS were tested.

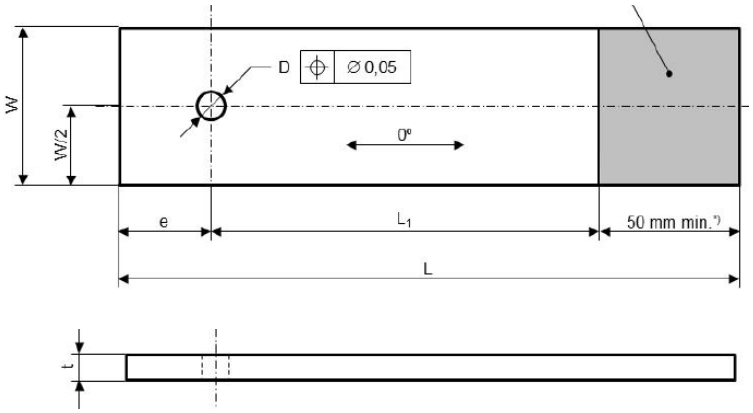

Fig 5-7 Test sample geometry

The table gives the dimension of a test sample for the bearing test. The system recordes the forces and displacement and calculates initial and ultimate bearing strength using the relations given below.

$$\sigma_{\mathrm{i}} = \frac{P_{\mathrm{i}}}{d\ t_{\mathrm{a}}}$$

$$\sigma_{\mathrm{u}} = \frac{P_{\mathrm{u}}}{d\ t_{\mathrm{a}}}$$

Where σ_i : Initial bearing strength (MPa)

σ_u : Ultimate bearing strength (MPa)

P_i : Load at initial peak point on bolt bearing curve (N)

P_u : Load at 6% deformation of the hole diameter (N)

d : bolt diameter (mm)

t_a : actual thickness of the sample (mm)

Table 5-3 Test sample geometry

Hole diameter d (mm)	Width w (mm)	Edge distance e (mm)	Sample length L (mm)	Bolt diameter (mm)	
				Min	Max
6.35	45±0.1	25±0.1	150	6.312	6.337

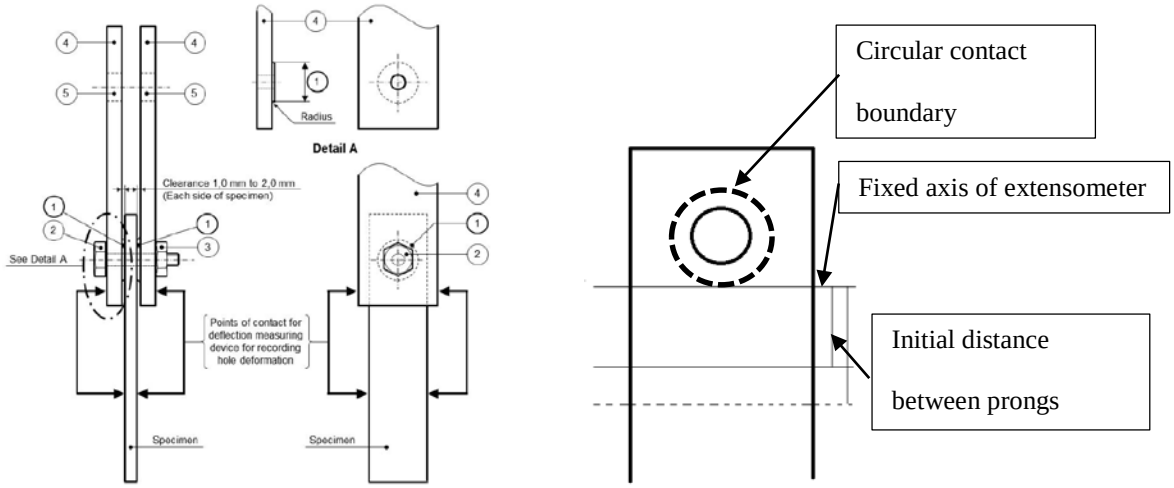

Fig 5-8 Clamped section on bearing specimen

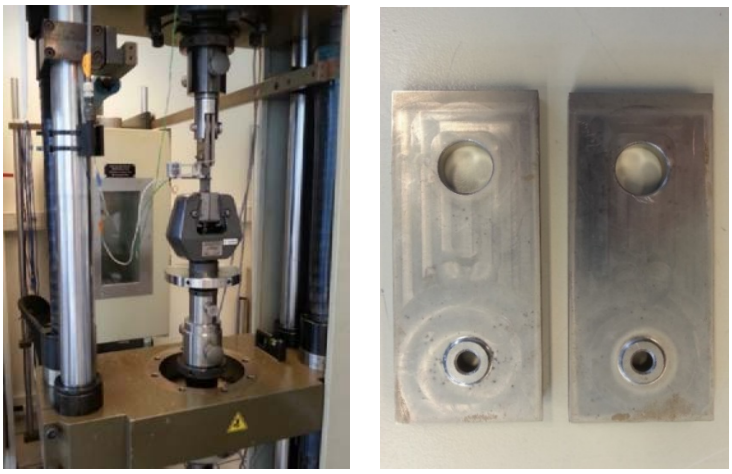

Fig 5-9 Test setup at TenCate and loading plates with bearing samples

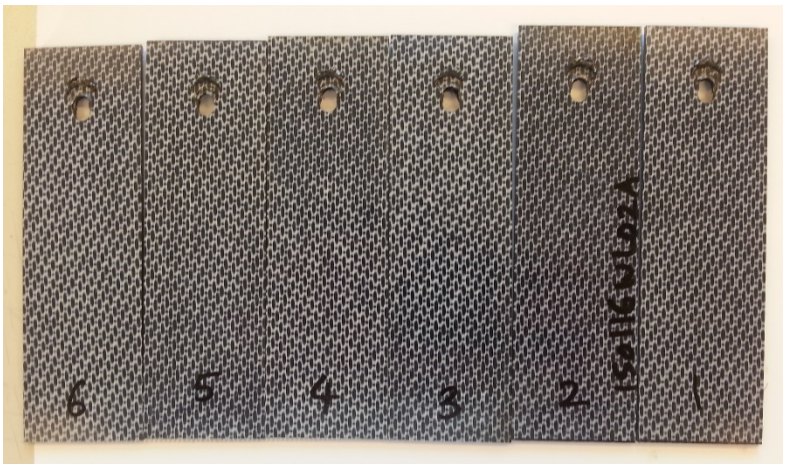

Fig 5-10 Bearing samples

CHAPTER 6. ANALYSIS

6.1 Flexural Strength

As we have seen from the literature review, the flexural strength of a laminate depends upon the constituent plies, their orientation and their position in the laminate structure. The [D] matrix represents the flexural stiffness of a laminate and reflects the change in flexural stiffness with change in thickness or orientation of the plies. There are various free softwares available which calculate the bending stiffness [D] matrix for different layup conditions.

Laminate analysis program (LAP) developed by Imperial College of London and based on classical laminate theory was used in this research to calculate the influence of orientation on the [D] matrix. The software takes the ply properties and orientation as inputs and calculates the ABD matrices for different layups. Since the software is designed for unidirectional plies, a woven fabric is entered as combination of two plies. For example a woven (0,90) fabric is entered as two different 0° and 90° unidirectional plies to simulate mechanical response. For hybrid 3, with discontinuous carbon-PPS flakes, the replacement layers are assumed to have quasi-isotropic layer properties.

Using this software, the change in the flexural response of the material with different layups can be studied. The inverse of $[D]^{-1} = [d]$ matrix gives the compliance of a laminate. Lower is the d_{11} term, higher is the flexural stiffness of the laminate structure.

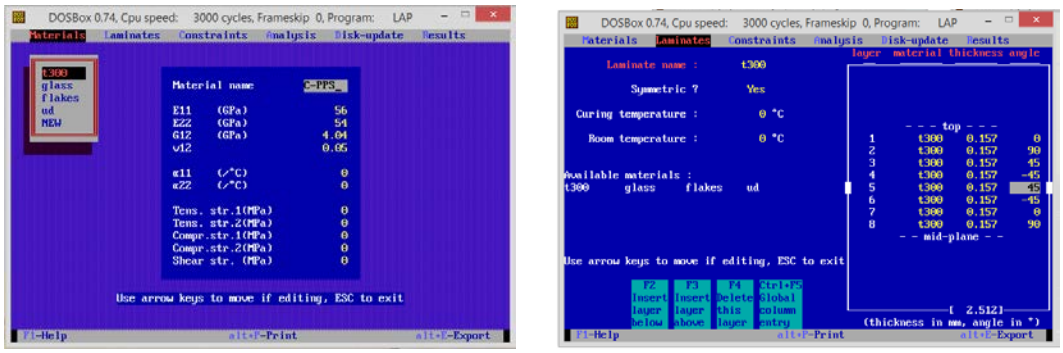

Fig 6-1 Input parameters for LAP software

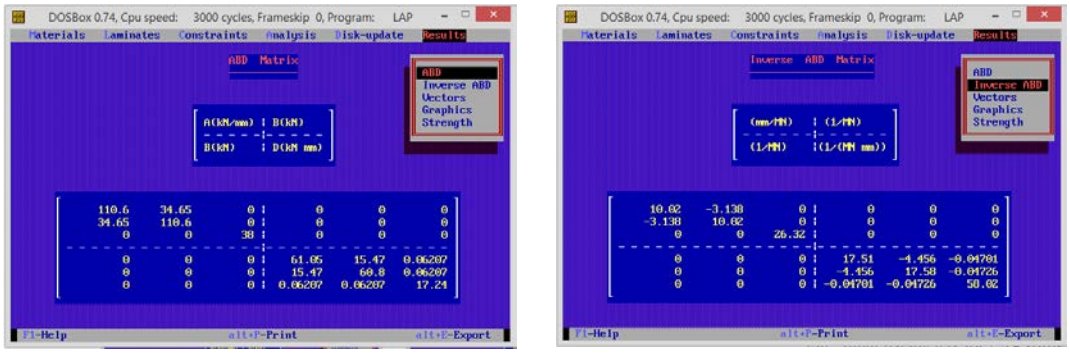

Fig 6-2 Output given by the LAP software

Using the software, the bending compliance for the chosen layup can be calculated for different hybrids and all-carbon-PPS and all-glass-PPS layup. For the chosen quasi-isotropic layup $[(0,90)/(\pm45)_2/(0,90)]_s$, the table shows how the flexural stiffness of a laminate decreases with replacement of layers near the mid-plane. Actual thicknesses of the manufactured laminates are used as input in the software.

The all carbon-PPS layup shows the lowest bending compliance which means it has the highest flexural stiffness. Hybrids 3 with discontinuous carbon-PPS flakes has the next lowest bending compliance followed by hybrid 1 and 2 with glass-PPS as center layers. The all glass-PPS has the highest bending compliance thus showing that it has the lowest flexural stiffness.

Table 6-1 Comparison of different laminates and their bending compliances

Type of laminates	d_{11} (1/ MN.mm)
Carbon-PPS	17.51
Hybrid 1	22.73
Hybrid 2	22.84
Hybrid 3	20.75
Glass-PPS	76.65

The experimental results of three point bend test gives the flexural strength and flexural modulus. However all the laminates have different thicknesses which makes it difficult to compare the flexural strength of these laminates with all carbon-PPS laminate. Therefore specific flexural strengths have been found by dividing the flexural strength of each laminate with its density. Since the density is a function of volume which in turn is a function of thickness, the comparison becomes possible as the differentiating parameter has been removed. The density of each laminate was calculated by weighing the laminate and dividing it by its volume.

From the table 6-2, it can be seen that the hybrids show comparable flexural strength and flexural modulus with respect to all carbon-PPS laminate.

Table 6-2 Specific flexural strength and flexural modulus for different laminates

Type of laminate	Specific Flexural Strength (N.mm/g)	Coefficient of variation (%)	Flexural modulus (GPa)	Coefficient of variation (%)
Carbon-PPS	464.19	1.8	43.06	2.78
Hybrid 1	449.82	2.9	42.64	1.43
Hybrid 2	464.10	4.21	43.04	6.43
Hybrid 3	439.11	6.22	42.78	5.18
Glass-PPS	251.56	13.3	23.77	2.75

This agreed with the previous findings [14] [16] about hybrids and highlighted the fact that inspite of having lower modulus material near the center, the flexural strength of the entire laminate is not affected much. The reduction in strength for glass hybrids 1 and 2 is less than 3% whereas for hybrid 3 with discontinuous carbon-PPS flakes it is 5%. The flexural modulus of the hybrids are very close to that of all carbon-PPS. The reduction in flexural modulus of the hybrids was approximately 1% of the flexural modulus of all carbon-PPS modulus. The all glass-PPS showed flexural modulus which was half of flexural modulus of all carbon-PPS laminate. Hence it was seen that carbon fibers dominate the flexural behavior of the hybrids 1 and 2.

A coefficient of variation (CV) under 5% means good repeatability is obtained in the results from different samples. With hybrid 2 the CV was higher than 5% which shows higher deviation in thickness of the samples tested. This was due to the resin flow during the consolidation and the uncertainty could be reduced by repeating the experiment again. Hybrid 3 showed higher coefficient of variation as well. For hybrid 3 it could have been due to non-homogenous distribution of flakes which results in greater scatter in the values.

Using the analytically obtained values of bending compliance, flexural modulus can be calculated and compared with experimentally obtained.

Table 6-3 comparison on flexural modulus values obtained analytically vs experimentally

Laminate	Flexural modulus (GPa) (using CLT)	Flexural modulus (GPa) (experimentally)
Carbon-PPS	43.25	43.06
Hybrid 1	45.77	42.64
Hybrid 2	43.50	43.04
Hybrid 3	45.80	42.78
Glass-PPS	24.85	23.75

The classical laminate theory tends to over predict the values of flexural modulus but not much difference was seen between the analytical values and experimental values. Thus the classical laminate theory gave a good prediction for the flexural modulus.

A graph of load vs displacement could be plotted for all laminates to compare the slopes of different hybrids. From the fig 6-3, it was seen that the hybrids have slopes between the all carbon-PPS and all glass-P. However the influence of carbon plies was higher hence the slopes of hybrids were closer to all carbon-PPS. It could be seen that hybrids 2 and 3 have almost similar slopes.

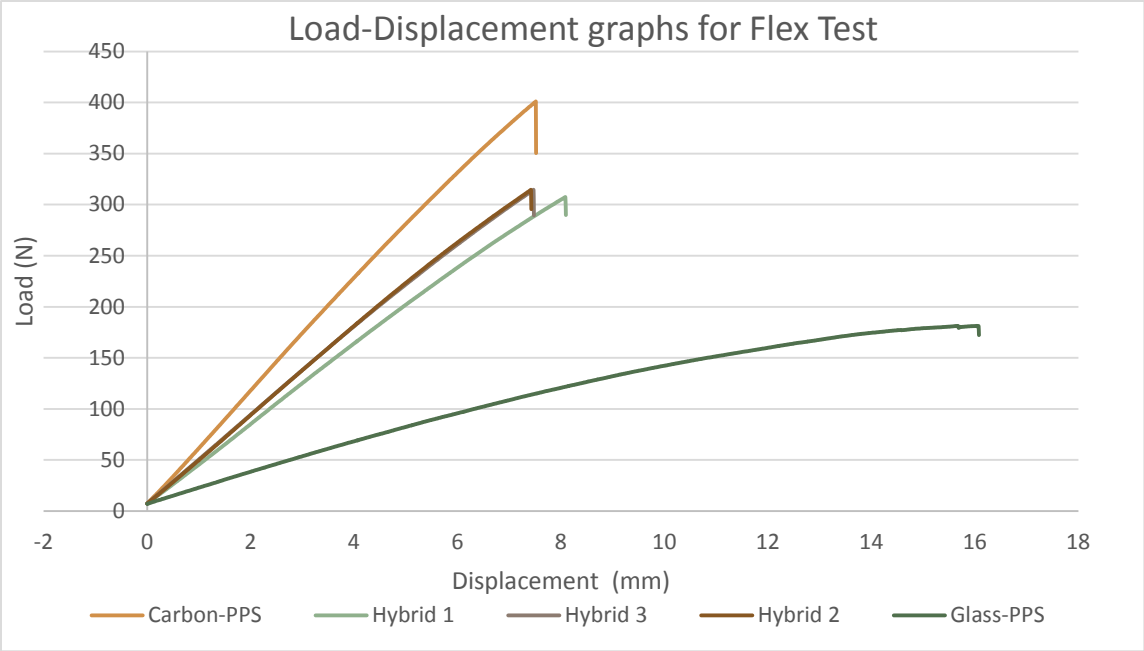

Fig 6-3 Load vs displacement graph for all the laminates

These results thus prove that for secondary structure applications with focus on flexural strength, the hybrids could be used as a replacement to the all carbon-PPS laminate structure.

6.2 Interlaminar Strength

The interlaminar strength was calculated using the Lekhnitskii solution [40] given in the standard. In the four point bend test, the sample was under pure moment and hence to find the stresses in radial and tangential direction of the sample, only the moment was

used. The stresses induced in the bend were independent of the angular position as the samples were under pure bending but depend on the radial position. The radial tensile stresses range from zero at the inner radius to a peak at the mid plane. Hence for curvatures in structures, the layers near the mid-plane in the laminate structure become crucial. The stresses induced in the samples are given in the table.

According to the experimental data, the carbon-PPS laminate showed the highest interlaminar strength and the glass-PPS showed the lowest strength. In hybrids 1 and 2 the effect of replacement of carbon plies with glass plies was clearly visible as the strength of the hybrids was only half of the strength of all carbon-PPS laminates. Also the failure mode changed from brittle and sudden failure in all carbon-PPS to gradual failure in hybrids. This behavior was similar to that shown by all glass-PPS laminate. For hybrid 1, the strength further reduced due to polyamide sizing on the glass fabric. This sizing showed low compatibility with polyphenylene sulfide and reduced the bonding strength between the glass and carbon plies.

Table 6-4 Interlaminar Strength and coefficient of variation for different laminates

Laminate	Interlaminar tensile strength (MPa)	Coefficient of variation (%)
Carbon-PPS	51.19	3.86
Hybrid 1	22.09	5.25
Hybrid 2	34.02	8.34

Sample	Interlaminar tensile strength (MPa)	Coefficient of variation (%)
Hybrid 3	40.45	4.77
Glass-PPS	16.29	7.80

For hybrid 3 with discontinuous carbon-PPS flakes, the failure is similar to carbon-PPS and its interlaminar strength reduces by 20%. The interlaminar strength for hybrid 3 was highly sensitive to the flake distribution as the response of the sample changed if there were flakes in the curvature or resin rich region. However even with non-homogenous distribution, a good repeatability was found in the results and the strength of laminates could be improved with improving the distribution of the flakes. A load-displacement graph was plotted for different laminates and the slopes were compared.

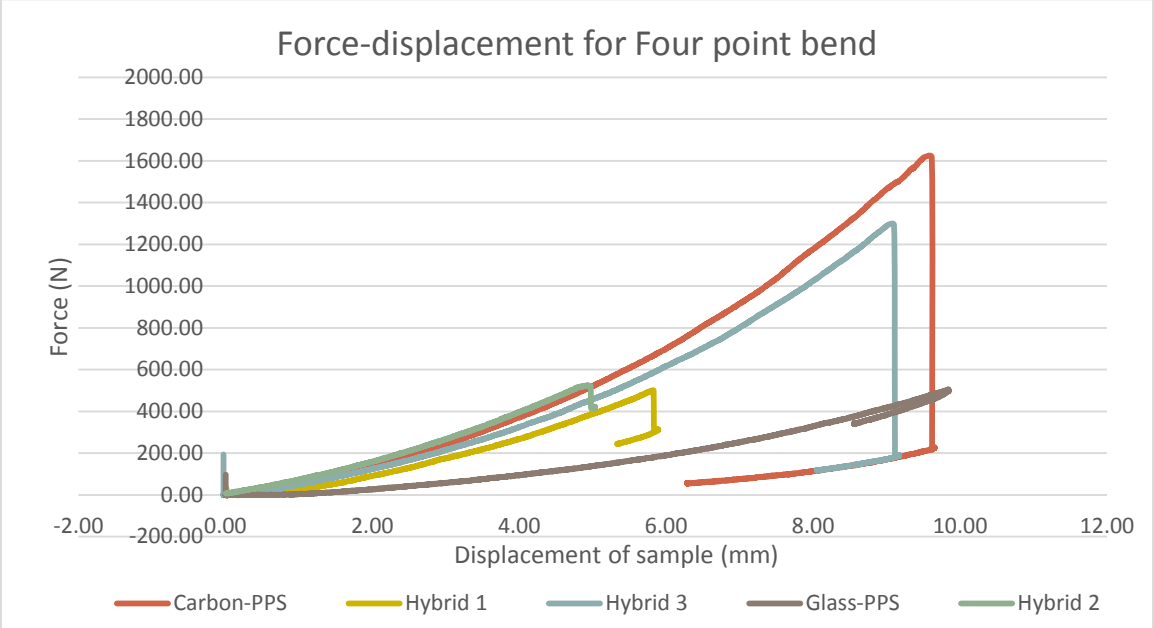

Fig 6-4 Force vs displacement for different laminates

The slopes of loading for all the laminates were continuous which concluded that no load drops were recorded. Load drops generally occur due to cracks or singularities present in the laminate sample formed during the reconsolidation. The failure in carbon-PPS sample was sudden with a load drop of 86% whereas for hybrids 1 and 2, the load drop was only 40%. Hybrid 2 showed similar behavior as all carbon-PPS laminate with 84% load drop and sudden failure. The load at the peak was also low for all the hybrids. However it was noted that higher was the peak load, greater was the load drop at the failure. This could be due to greater strain energy released during the failure of the laminates.

Thus it can be concluded that for application of secondary structures with focus on interlaminar strength, replacing the layers near the mid-plane with glass layers reduces the strength drastically. Hybrid 3 with discontinuous carbon-PPS flakes can be a better alternative to all carbon-PPS laminates.

6.3 Bearing Strength

Bearing failure can be compared to localized compressive failure at the contact between the bolt and hole edge in the laminate. It is highly sensitive to the ply structure and compressive material properties. Hence to compare the changes in the bearing response of the hybrids with respect to all carbon-PPS laminate, bearing test was performed.

All the laminates achieved an initial peak before experiencing a reduction in strength and increasing again to achieve the ultimate peak before complete failure. The initial peak marks the end of linear response of the material. Therefore it was important to note the

initial peak strength as well as the ultimate peak strength. Also as the thicknesses of the different hybrids were different, the bearing strength was divided by density (Specific bearing strength) to give a better comparison. Table shows the values recorded during the experiment.

Table 6-5 Initial bearing strength and specific bearing strength for different laminates

Laminate	Thickness (mm)	Initial Bearing strength (MPa)	Specific Bearing strength (N.mm/g)	Standard Deviation (MPa)
Carbon-PPS	2.512	371.63	238.22	30.11
Hybrid 1	2.276	359.54	216.59	12.74
Hybrid 2	2.330	426.22	268.06	9.80
Hybrid 3	2.337	443.80	269.29	52.02

Table 6-6 Ultimate Bearing strength and specific bearing strength

Laminate	Thickness (mm)	Ultimate Bearing strength (MPa)	Specific bearing strength (N.mm/g)	Standard deviation (MPa)
Carbon-PPS	2.51	619.86	397.35	27.05
Hybrid 1	2.27	601.70	362.47	47.98
Hybrid 2	2.33	652.65	415.84	35.00
Hybrid 3	2.34	685.30	410.47	68.86

From the tables 6-5 and 6-6 it was seen that hybrid 2 and hybrid 3 showed higher initial and ultimate bearing strength than the all carbon-PPS laminate. Hybrid 1 showed a reduction of 3% in ultimate bearing strength and initial bearing strength. This reduction in strength could be partly due to incompatible sizing on the glass fabric which causes stresses to build up during consolidation. These stresses provide a nucleus for crack formation and propagation. Since hybrid 2 with compatible fabric sizing showed higher bearing strength, it could be concluded that the reduction in strength was not only due to replacement glass fabric. However hybrid 1 still displayed comparable bearing strength as compared to all carbon-PPS laminate.

The increase in the bearing strength for hybrid 2 could be attributed to fiber bridging in the hybrid laminate. According to Kardomateas [41], fiber bridging in polymeric composites is a source of considerable toughness. The concept of fiber bridging a crack can be explained as a crack opening which is small enough to be accommodated by enhanced extension of the fiber located near it. As the crack opening gets wider, the fibers experience fiber pullout or complete failure. The matrix cracks formed in the sample are bridged by the fibers over it. Kretsis [14] concluded that the increase in strength of hybrids is due to breaking of low elongation fiber system (higher modulus fiber) and the high elongation fiber system taking up the load after that to give additional strength to the laminate.

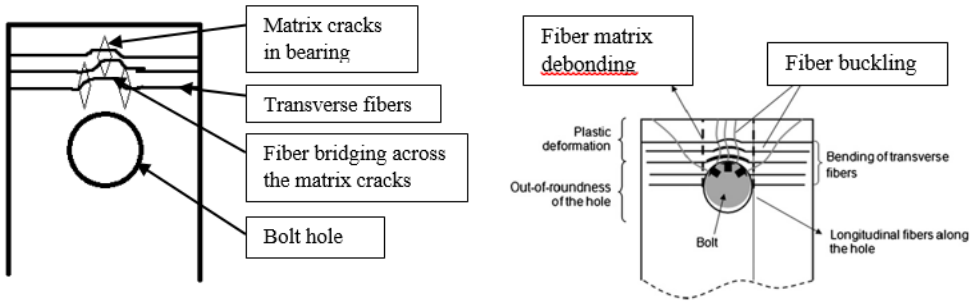

Fig 6-5 Fiber Bridging and buckling for bearing failure

Hybrid 3 showed an increase of 15% in initial bearing strength and nearly 6% in ultimate bearing strength. The randomly oriented discontinuous carbon-PPS flakes act as quasi-istropic layer creating a network of fibers in mulitple directions. Generally quasi-isotropic layup in woven fabrics is found to increase the bearing strength of a laminate [29]. However the non-homogenity affects the data and resulted in higher scatter and utimately higher factor of safety in the end design. This needs to be reduced for hybrid 2 to be used in structural applications.

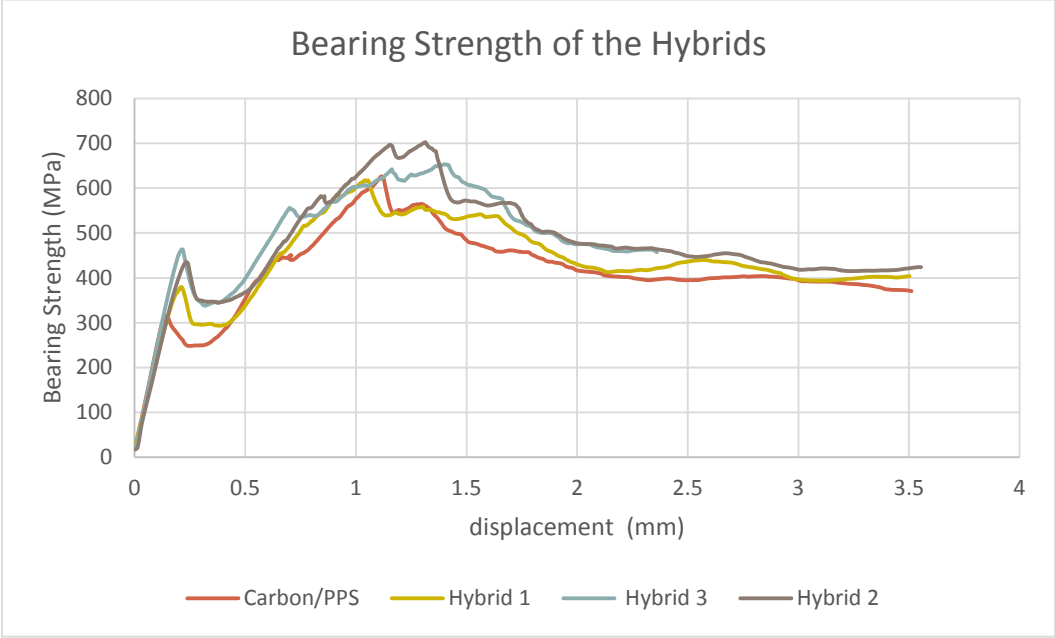

Fig 6-6 Bearing strength vs displacement in different laminates

The graph (figure 6-6) shows the behavior of different laminates under bearing load. It was seen that all the hybrids showed higher strengths than the base all carbon-PPS laminate. Also for the hybrids it was noticed that the drop in load after the initial peak is less than all carbon-PPS laminates. After the load drop the hybrids showed similar load behavior as the carbon-PPS laminate. The hybrids continue to carry higher loads and ultimately failed at higher loads than all carbon-PPS laminate.

Therefore it could be said that hybrids show increased bearing strength and could be a great potential for structures with bearing failure as critical design parameter.

CHAPTER 7. MICROSCOPY

7.1 Sample Preparation

To observe the failure type and pattern within the test samples, the samples were cut along their failure zone. The cut specimens were immersed in a mixture of epoxy and hardener and cured overnight. The epoxy samples were then polished and observed under an optical microscope. An Olympus BHM (Japan) optical microscope coupled with Sony CCD-IRIS hi resolution system was used to record the microscopy images.

Fig 7-1 Epoxy-Hardener system and samples cured in the mixture

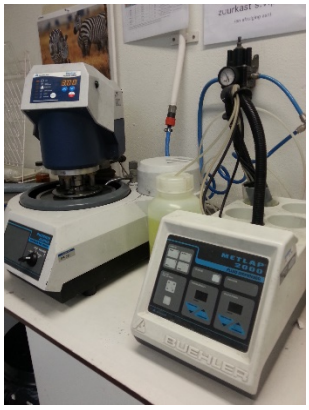

Fig 7-2 Automatic polisher (Bubhler vector power head and phoenix alpha grinder)

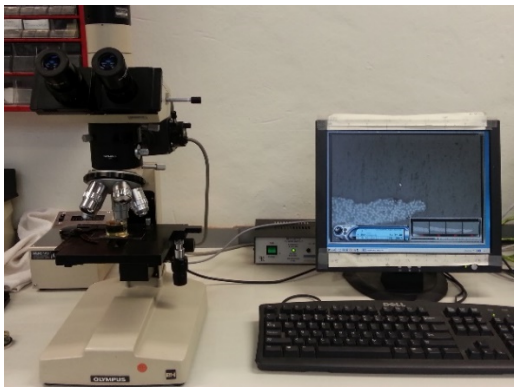

Fig 7-3 Olympus microscope coupled with Sony video camera system

7.2 Failure pattern in flexural test samples

In the all carbon-PPS laminate, the failure mode during flexural test was seen as compressive and tensile failure in the surface plies. The span-to-depth ratio used in this research is 39:1. In three point bend test, presence of shear stresses is inevitable. However for a large span-to-depth ratio as used in this research, the shear effects are minimized and are not the main modes of failure.

It is very difficult to predict which mode of failure occurred first from microscopy as the failure is sudden and final. The cracks originate in the surface (0,90) layer and cause further delamination between the (0,90) and (±45) ply.

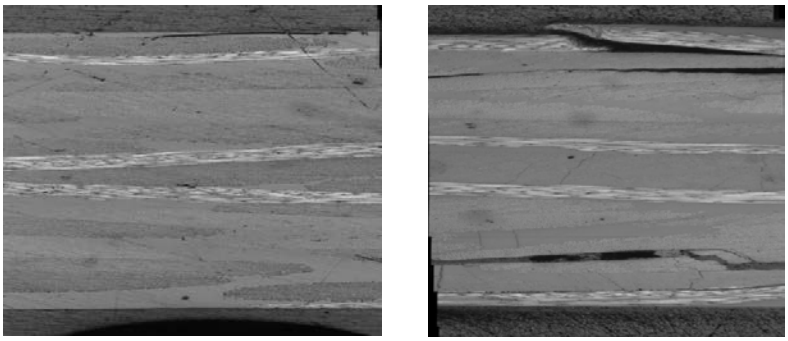

Fig 7-4 Carbon-PPS before and after the test

To experimentally find the first failure mode, the test was stopped at subsequent displacements and microscopy was done. However no cracks were seen through the laminate until the final fracture. The progression on stress through the laminate could be found using finite element method which will be the future of this project.

For hybrids 1, 2 and 3, similar failure pattern was observed on microscopy. The failure started at the surface plies and the delamination spread through the subsequent plies. For hybrids 1 and 2, the delamination was seen to occur between the (0,90) ply and (±45) ply along with delamination between the two (±45) plies as well. For hybrid 3, delamination was limited to (0,90) and (±45) layer.

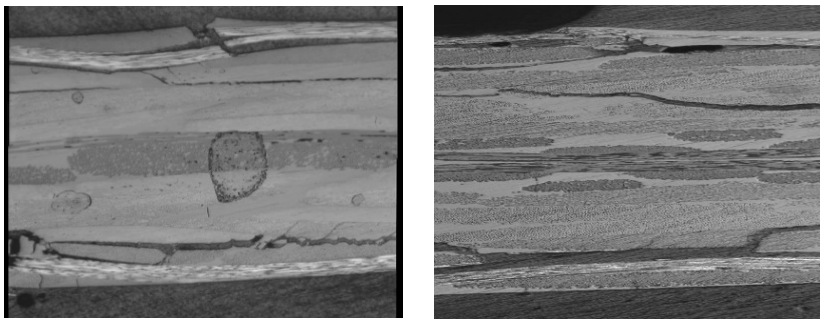

Fig 7-5 Failure in Hybrid 1 and Hybrid 2

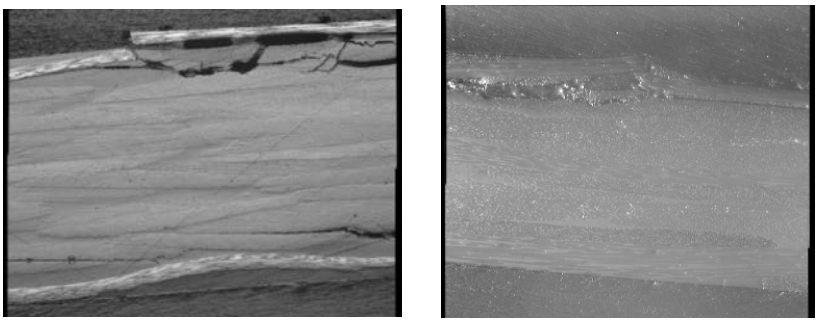

Fig 7-6 Failure in Hybrid 3 and glass-PPS laminate

The glass-PPS laminate failed in compression with a large displacement. The failure was gradual and the fibers elongated a lot before causing ultimate failure. However the hybrids did not exhibit this behavior which showed that the outer carbon-PPS layers dominate the failure behavior. This agreed with previous literature on hybrids [14]. Hence the hybrids can be used as possible replacement to all carbon-PPS laminate.

7.3 Failure pattern in interlaminar strength test samples

The interlaminar strength of hybrid laminates was evaluated by performing four point bend test on a 90° curved sample for different laminates. As the sample was in pure moment, it was seen that delamination was the major mode of failure in the samples. The delamination was observed to begin at the center of the curvature and then gradually spread to the legs of the sample.

The all carbon-PPS laminate failed suddenly at ultimate load. Multiple cracks were observed in all carbon-PPS sample with multiple branches and gave a shattered appearance.

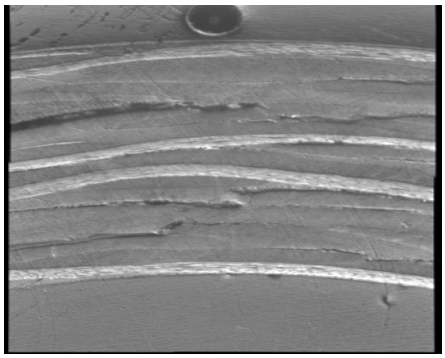

Fig 7-7 Carbon-PPS laminate after failure

The major delaminations were observed in (±45) plies and between the (0,90) ply in the center and (±45) ply. Some of the cracks were seen traversing the ±45° ply along the tow boundary. The multiple cracks could be attributed to higher failure load causing greater release of energy.

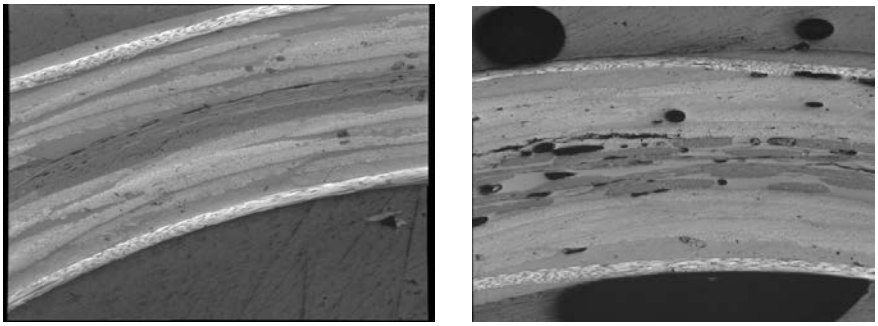

Fig 7-8 Failure in hybrid 1 and hybrid 2

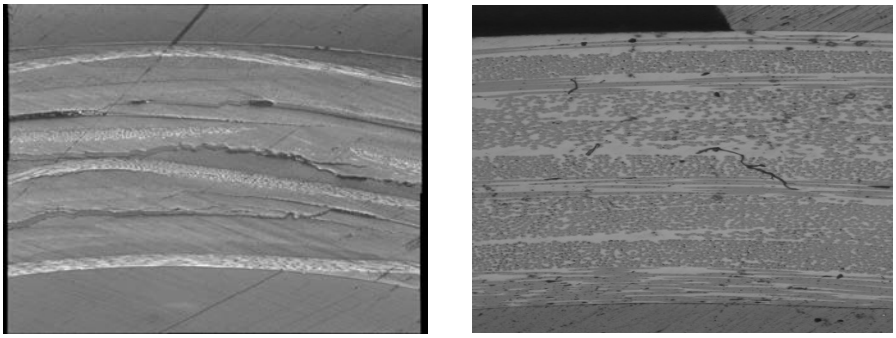

Fig 7-9 Failure in hybrid 3 and glass-PPS

For hybrid 1 the delamination was concentrated along the ply boundary of carbon and glass plies. The damage pattern was not scattered like all carbon-PPS and only a single crack was seen. This delamination could be due to the different poission ratio of the different materials. Similar phenomenon was noticed in hybrid 2 where delamination is seen between the glass and carbon ply. However in the case of hybrid 2, the cracks extended within the glass layers and delaminations were seen within the two center glass plies as well. The interlaminar strength of hybrids 1 and 2 was found to be much closer to the interlaminar strength of all glass-PPS which shows that the center glass layers dominate the failure mode. The failure in glass-PPS was difficult to observe. The failure was gradual and along the center of the laminates, it fails ultimately. The layers move back after the load has been released and hence the cracks were not readily visible.

Hybrid 3 mimicked the failure pattern of all carbon-PPS laminate with a shattered crack appearance. Multiple cracks were seen through the thickness of the laminate with major delaminations concentrated between the (±45) plies and in the flake layer. The cracks were seen travelling through the resin rich areas in the discontinuous carbon-PPS flakes layer. However hybrid 3 showed the highest interlaminar strength among the hybrids and the strength may improve with higher homogenity in the discontinuous carbon-PPS flakes dstribution.

7.4 Failure pattern in bearing test samples

The laminates attained an initial peak, saw a reduction in strength and again increased in strength to fail at higher loads.

At the initial peak, the tow in immediate contact of the bolt have been damaged and load gets transferred to the resin. According to Vieille et al [36], as the hole deformation increases, the load gets carried by the undamaged 0° fibers in the (0,90) plies in the center and the surrounding (±45) plies surrounding them. Ultimately the tows undergo the same failure mechanism and lead to extended damage of the bolt hole.

The washer region of the test setup clamps the sample and prevents the out of plane deformation of the plies as shown in fig 7-10. However in the region above the washer, out-of-plane deformation was seen and was instrumental in releasing some of the energy applied to the laminate [34].

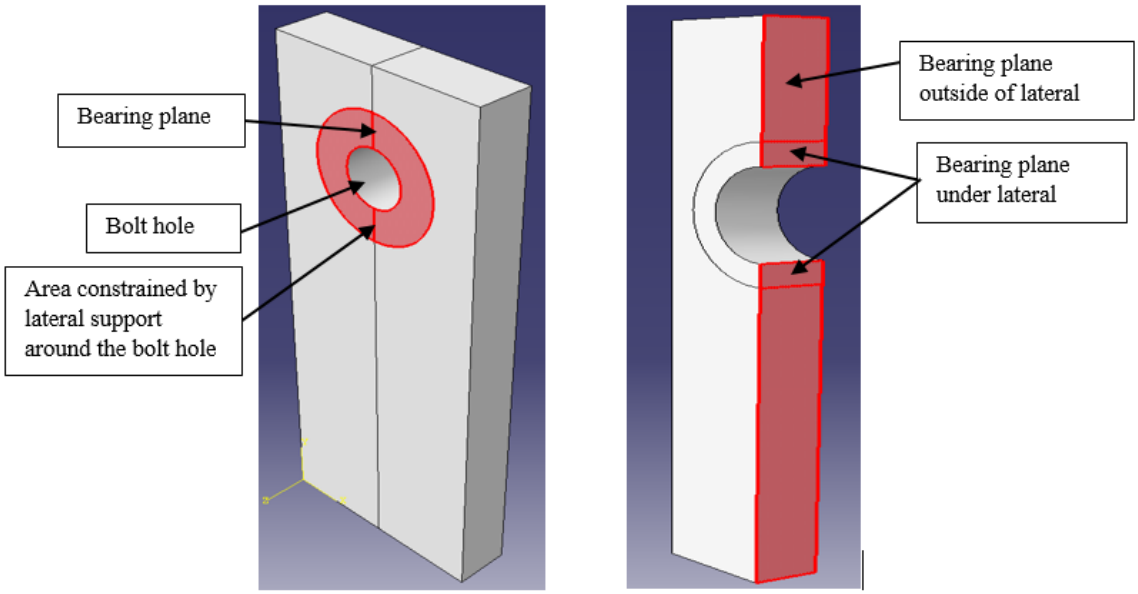

Fig 7-10 Constrained region on laminate and Bearing plane in a sample

The laminate was cut along the bearing plane and the quarter above bolt hole was dipped in epoxy. The section was studied under microscopy for the damage pattern. Sometimes the damage begins from the cracks and abrasions left inside the hole circumference while drilling. To make sure that the sample did not have any major damage before test, the circumference of the hole was observed under a microscope.

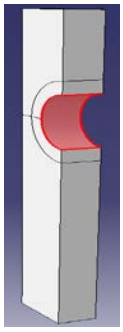

Fig 7-11 Hole circumference observed under the microscope

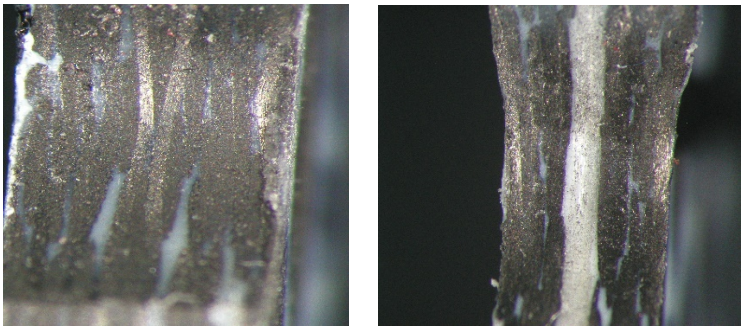

Fig 7-12 Circumference region for carbon-PPS and hybrid 1

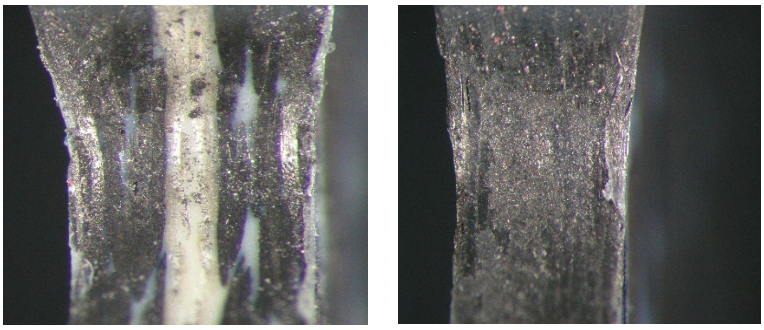

Fig 7-13 Circumference region for hybrid 2 and hybrid 3

From the figs 7-12 and 7-13, no major damage was seen during drilling the hole and wasn't a cause for any major failure. The microscopic images for damage at initial peak in different laminates are given by figs 7-15 and 7-16.

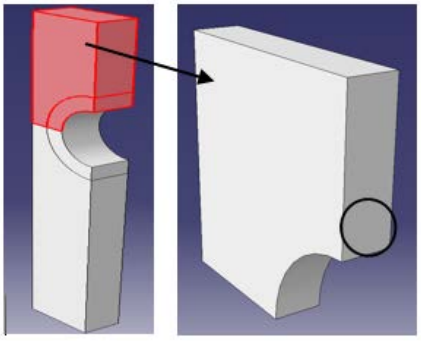

Fig 7-14 Location of microscopic images

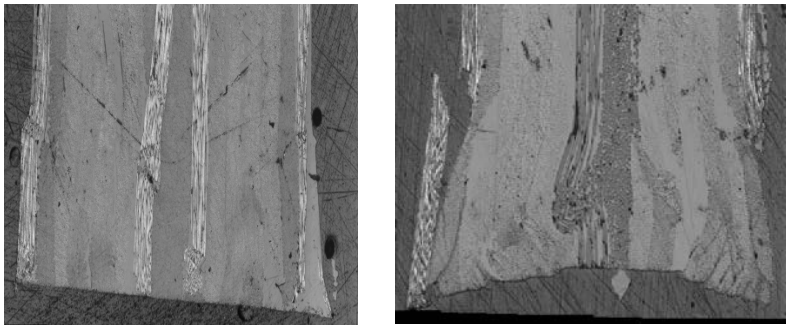

Fig 7-15 Initial peak for carbon-PPS and hybrid 1

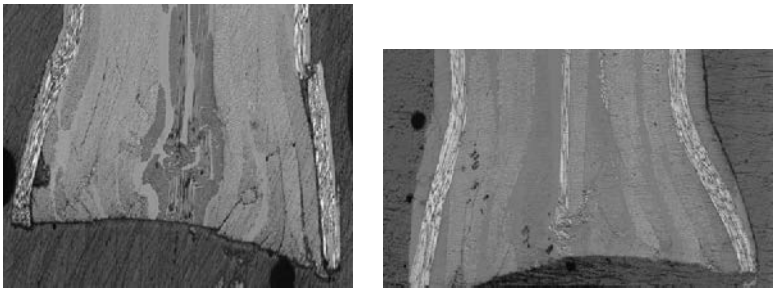

Fig 7-16 Initial peak for hybrid 2 and hybrid 3

For all carbon-PPS, the fiber microbuckling was seen in the 0° fibers in (0,90) in the center of the laminate and on the surface. A few matrix cracks were seen in (±45) plies surrounding the center plies. In hybrid 1, the glass fibers showed fiber splitting. Along with this, matrix cracks were observed between the glass and carbon plies. The glass fabric at the center seemed to have undergone plastic deformation and resulted in deformation. Hybrid 2 also showed similar behavior with cracks within the glass plies and delamination and shear cracks in (±45) plies. The glass plies were seen to deform from the point where the bolt came in contact with the laminate.

In hybrid 3 the discontinuous carbon-PPS flakes oriented in 0° showed fiber kinking. Shear cracks were seen to originate from the contact edge into the (±45) plies. However as compared to other hybrids, hybrid 3 showed least amount of damage at the initial peak. At final failure, greater amount of damage is seen in the laminates.

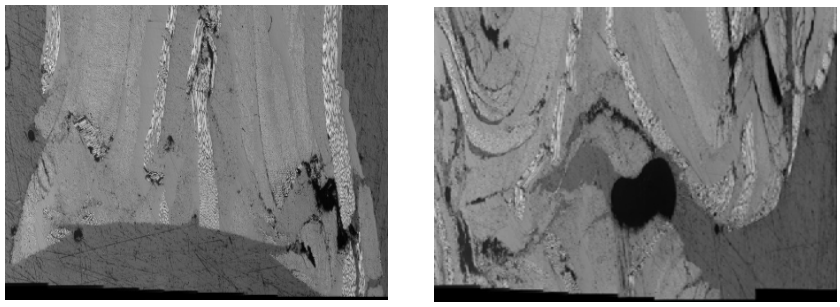

Fig 7-17 Damage at ultimate load in carbon-PPS at the hole edge and at washer edge

At the final failure, the fiber buckling was enhanced along with shear cracks at the edge of hole. The shear cracks caused large scale delamination to the outer surface plies and caused rapid disintegration. At the washer's edge the fibers experienced out of plane deflection which completely destroyed the laminate structure.

The hybrid 1 showed enhanced delamination between the (±45) plies with shear cracks running at 45° to the fiber direction. These shear cracks have caused the laminate to almost break apart.

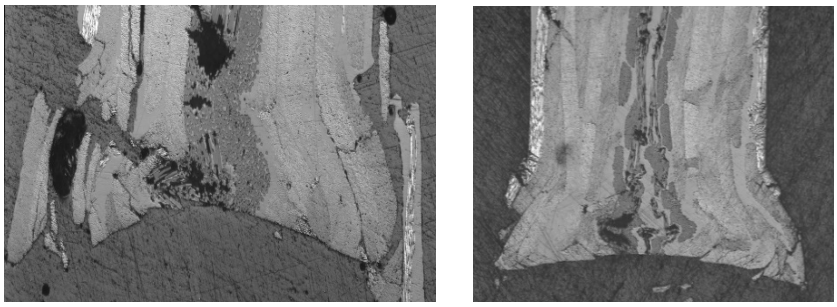

Fig 7-18 Ultimate failure in hybrid 1 and hybrid 2

A large delamination crack was seen in the center of the glass ply and it opened up due to the compressive forces. Hybrid 2 showed delamination cracking within the glass layers and between the glass and carbon layers. Delamination was also seen in the surface plies with cracks spreading into (±45) plies. From the microscopic images it was seen that fiber kinking, shear cracks and delaminations dominate the failure modes.

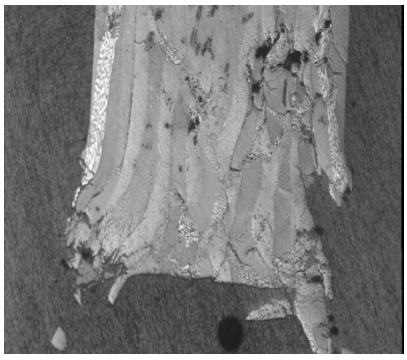

Fig 7-19 Ultimate failure in hybrid 3

In hybrid 3, the higher bearing strength was attributed to random orientation of the discontinuous carbon-PPS flakes. Major shear cracks were seen along the boundary of flakes through the matrix. These shear cracks induced delaminations along the (±45) plies leading to failure. Some portions of the surface plies were seen to break away from the laminate.

7.5 C-scans

In hybrid 3, it was seen that the initial bearing strength of the laminate depends on the discontinuous carbon-PPS flake distribution around the bolt hole. To find how the distribution of flakes affected the bearing strength, c-scans of the test samples were done.

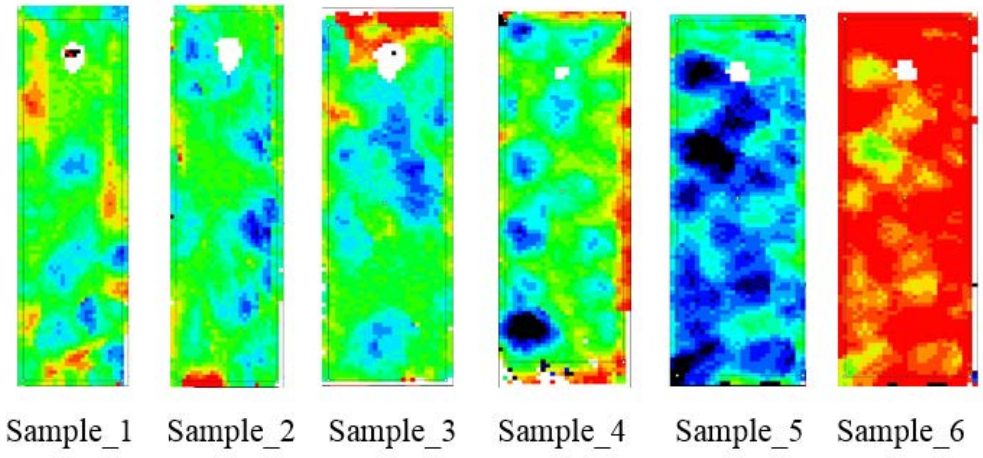

Fig 7-20 C-scans of bearing test samples showing flake distribution

Fig 7-21 Thickness scale for samples 1 to 5 and thickness scale for sample 6

Table 7-1 Different samples and respective initial bearing strength

Sample no	Initial Bearing strength (MPa)
1	350.8
2	463.6
3	432.8
4	457.7
5	417.6
6	389.9

The c-scan maps the thickness profile of the test sample. This helps in identifying the outline of flakes in the sample. Higher thickness means larger concentration of flakes and blue means lower flake content (higher resin rich area). The areas marked with green show areas of uniform thickness (atleast one flake). For sample no 6 since the thickness was beyond the scaling capacity of the machine, a new scale had to be adopted to show the flake concentration. The table 7-1 gives the corresponding initial bearing strength for different samples.

Sample 2 showed an uniform distribution of flakes around the bolt and hence highest initial bearing strength was observed. Sample 4 showed the next highest bearing strength with homogenous distribution of flakes. A homogenous layer of flake was observed in sample 4 (depicted by green colour) with a uniform distribution of resin areas. This helped in transfer of stress among the flakes and increased the bearing strength.

Sample 1 showed the lowest initial bearing strength. From the c-scan, resin pockets were observed above the bolt. This may have caused lower resistance to deformation and hence the sample showed poor bearing response. Sample 3 showed highest concentration of flakes above the bolt hole and showed second lowest bearing strength. The higher concentration of flakes caused a region of high fiber volume and reduced resin concentration. This in turn caused poor transfer of stress throught the laminate and early failure.

Hence it was be concluded that bearing strength of the laminates depend on the distribution of discontinuous carbon-PPS flakes and higher bearing strengh can be achieved with better dstribution.

CHAPTER 8. CONCLUSION

This research project was aimed at exploring the possibility of using the inter-ply hybrids in secondary structures as replacement of existing carbon-PPS structures. The hybrids provide a cheaper alternative and display similar characteristics to the all carbon-PPS laminate.

For flexural response, all three hybrids showed comparable flexural strength and rigidity. This supported the literature [14] [16] that state that the flexural response of the hybrids is dominated by surface plies and replacement of core layers have a small effect on the overall strength of the laminate. The position of the layers that are replaced and their orientation also affected the rigidity of the laminate.

The interlaminar response of the laminate in curved sections was dominated by the strength of the plies near the mid-plane of a symmetric laminate. Hence hybrids 1 and 2 showed poor performance and showed failure strength almost similar to all glass-PPS laminate. The bonding of the carbon plies to glass plies also became an important factor and hence the sizing of the fabric should be compatible to the resin system used. Hybrid 3 showed better interlaminar response but this could be increased with more homogeneity in flake distribution.

All the hybrids showed higher bearing strength than the all carbon-PPS laminate. The improvement was seen in both initial bearing strength and ultimate bearing strength. Both the glass fabric hybrids showed consistent higher bearing response than all carbon-PPS laminates. This proved that with any type of glass fabric having compatible sizing and good consolidation, the laminate will mostly show higher bearing strength. For hybrid 3 the effect of flake distribution on bearing strength was investigated using c-scans and it was found that higher bunching of flake caused a region of low resin content which reduced the overall bearing strength. Resin rich pockets above the bolt hole also reduced the overall bearing strength. Hence it is important to control the distribution of the flakes to get same response from multiple carbon-PPS flakes laminates.

Thus, from the overall report it can be concluded that thermoplastic hybrids provide a comparable alternative to carbon-PPS laminates and further research is needed to bring these hybrids into mainstream manufacturing for secondary structures.

CHAPTER 9. FUTURE RESEARCH

To further investigate the possibility of using discontinuous carbon-PPS flakes into aerospace structures, further research was carried out at Purdue University. TenCate Advanced Composites kindly provided the carbon-PPS semi-preg material for further research. Carbon-PPS and hybrid 3 type laminates were again created using the hot press at composite materials laboratory at Purdue University using the same press cycle as used at TenCate Advanced Composites, Netherlands.

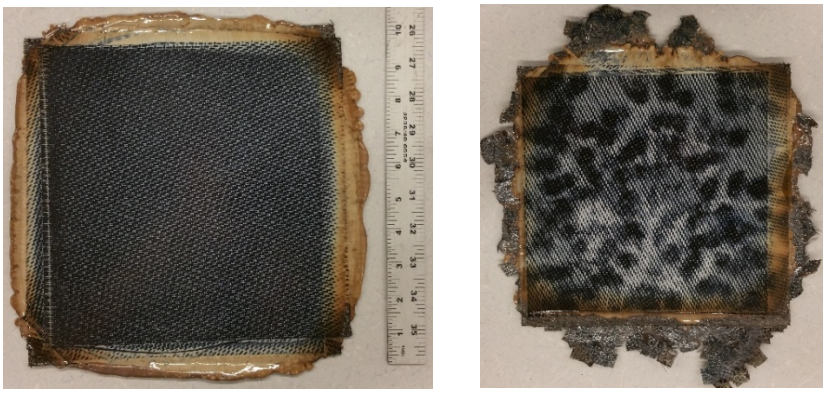

Fig 9-1 Carbon-PPS and hybrid 3 laminate at Purdue University.

Fig 9-2 Hot Press and Flat mold at Purdue University

The samples were then tested for flexure response to verify if the results differ from those obtained at TenCate. This was done to note the influence of manufacturing environment on the quality of the laminate. Three point bend test was performed to evaluate the flexural strength of the samples.

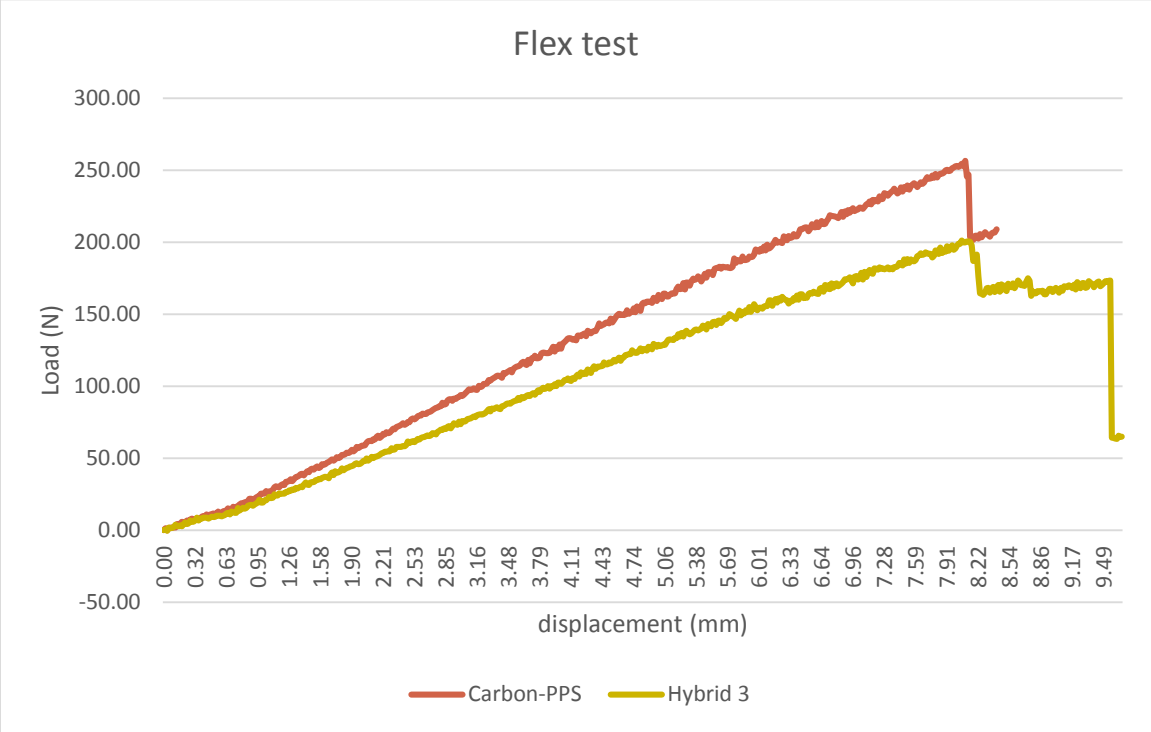

Fig 9-3 Load vs displacement for carbon-PPS and hybrid 3

From the grpah it was seen that the slopes of carbon-PPS and hybrid 3 were close and both the laminates showed same displacement before ultimate failure. The hybrid showed deviaiton from the carbon-PPS due to non-homogenous flakes. These results corresponded the results shown by the laminates made at TenCate. Hence it can be said that same laminate manufacturing conditions were simulated at Purdue University. Although the hybrid 3 shows higher flexural modulus, it is mainly due to reduced thickness. The reduction in thickness is a result of large of amount of flakes flowing out

of the laminate with resin during the manufacturing process. One area of future research is to devise technique to contain the flakes within the mold during manufacturing and ensure its homogenenity throughout the laminate.

Table 9-1 Flexure test data for carbon-PPS and hybrid 3

Laminate	Thickness (mm)	Flexural modulus (GPa)
Carbon-PPS	2.17	42.59
Hybrid 3	1.94	48.75

Another area of future research for this project was understanding the mechanism of failure in curved laminates under pure bending. To manufacture the curved sections, a thermoforming system is to be setup at Purdue University. The mold has been designed and manufactured and the electrical systems have been setup. All the components will be assembled to make the complete thermoforming system. Using this, the delamination mechanism in the hybrid curved laminates and its influence on the flake distribution can be studied in the future.

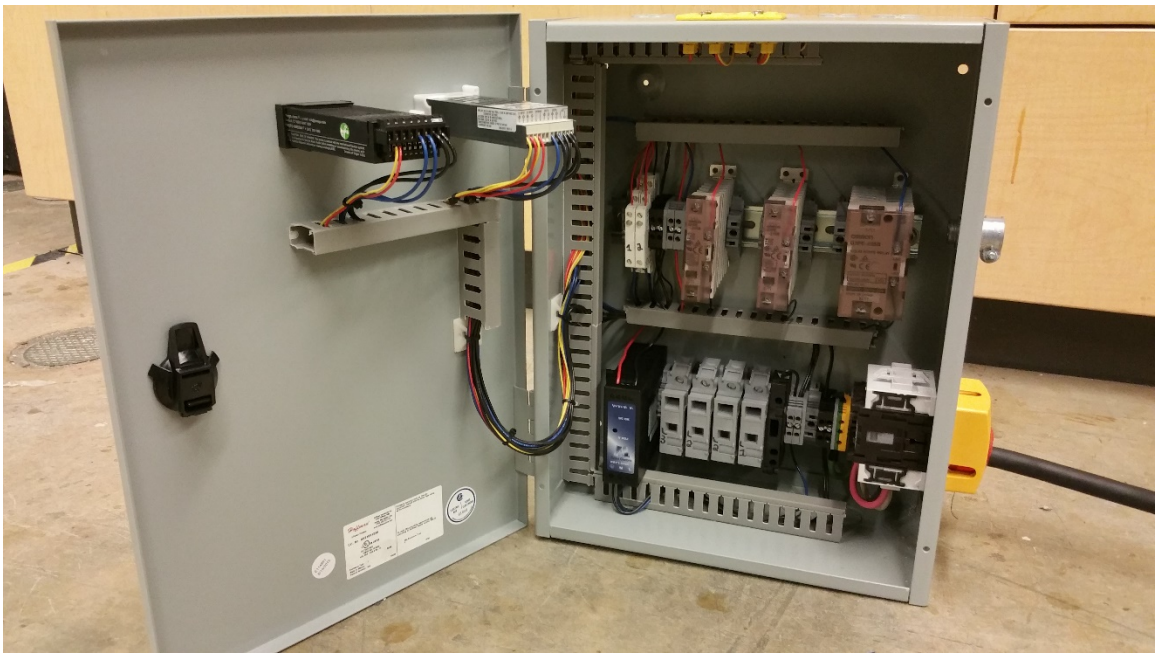

Fig 9-4 Electrical circuits for the thermoforming system

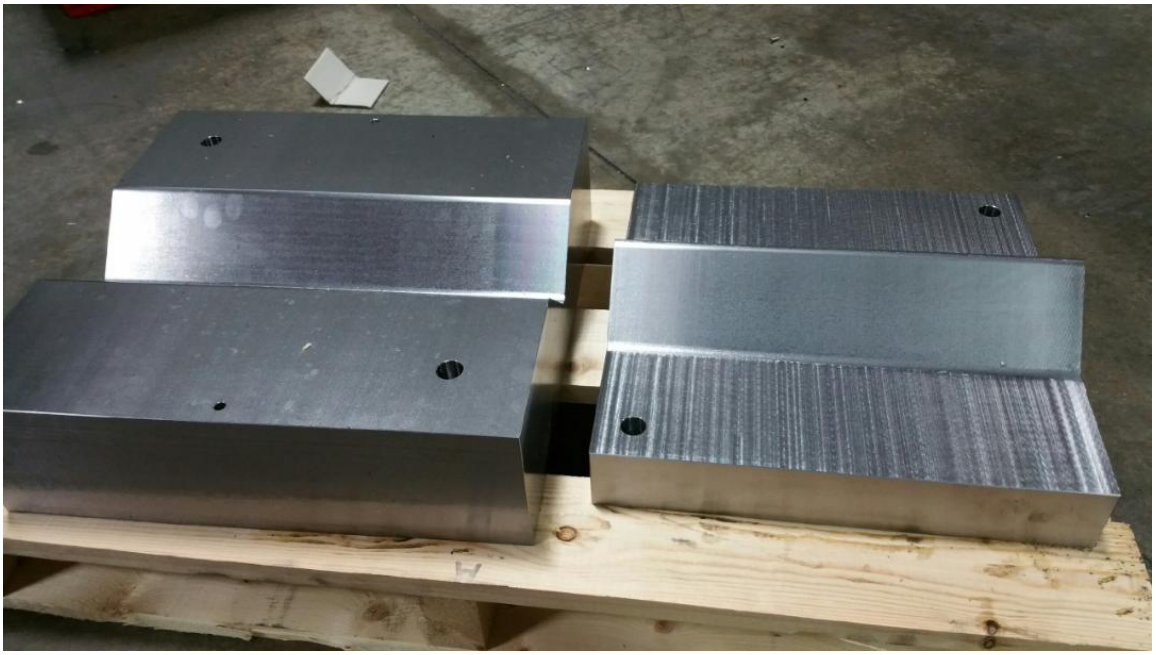

Fig 9-5 V-shape mold for angle parts

LIST OF REFERENCES

LIST OF REFERENCES

[1] C. Red, "The outlook for thermoplastics in aerospace composites, 2014-2023," 01 09 2014. [Online]. Available: http://www.compositesworld.com/articles/the-outlook-for-thermoplastics-in-aerospace-composites-2014-2023.

[2] N. Bombourg, "Reportlinker adds Opportunities in continuous fiber reinforced thermoplastics: 2009-2014," PR Newswire Association LLC, New York, 2009.

[3] C. Red, "High performnce composites," 1 September 2014. [Online]. Available: http://www.compositesworld.com/articles/the-outlook-for-thermoplastics-in-aerospace-composites-2014-2023.

[4] G. Marsh, "Reinforced plastics, the next wave?," Materialstoday, 4 August 2014. [Online]. Available: http://www.materialstoday.com/composite-applications/features/reinforced-thermoplastics-the-next-wave/. [Accessed 4 August 2014].

[5] F. technologies, "New Evolution; Progress in thermoplastic composites," Fokker Aerostructures, The Netherlands.

[6] "UL Prospector," UL, [Online]. Available: http://plastics.ulprospector.com/generics/41/polyphenylene-sulfide-pps.

[7] P. Mallick, Fiber Reinforced Composites, Marcel Dekker Inc, 1993.

[8] G. Marsh, "reinforced thermoplastic, the next wave ?," *Reinforced Plastics*, 04 August 2014.

[9] V. M. E. Vasiliev, "Fabric Layers," in *Advanced Mechanics of Composite materials and Structural elements*, Elsevier, 2013, pp. 223-225.

[10] "Advanced Composite Materials," FAA .

[11] D. Gurit, "Woven Fabrics," Gurit , 2011. [Online]. Available: http://issuu.com/gurit/docs/guide_to_composites/37?e=1086841/1088243.

[12] S. Black, "Thermoplastic composites "clip" time, labor on small but crucial parts," 30 April 2015. [Online]. Available: http://www.compositesworld.com/articles/thermoplastic-composites-clip-time-labor-on-small-but-crucial-parts.

[13] Y. Swolfs, L. Gorbatikh and I. Verpoest, "Fiber Hybrodosation in polymer composites: A review," *Composites Part A: Applied Science and Manufacturing*, no. 67, pp. 181-200, 2014.

[14] K. G, "A review of tensile, compressive, flexural and shear properties of hybrid fiber-reinforced plastics," *Composites*, vol. 18, no. 1, pp. 13-23, 1987.

[15] I. Kalnin, "Evaluation of unidirectional glass-graphite fiber/epoxy resin composites," *Composite Materials: Testing and Design* , vol. ASTM STP 497, pp. 551-563, 1972.

[16] J. Zhang, K. Chaisombat, S. He and C. Wang, "Hybrid composite laminates reinforced with glass/carbon woven fabrics for lightweight load bearing structures," *Materials and Design* , vol. 36, pp. 75-80, 2012.

[17] S. Black, "CompositesWorld," 1 March 2008. [Online]. Available: www.compositesworld.com/articles/aligned-discontinuous-fibers-come-of-age. [Accessed 1 March 2008].

[18] D. D. Howell and S. Fukumoto, "Compression molding of long chopped fiber thermplastic composites," in *CAMX - The Composites and Advanced Materials Expo,* Orlando, FL, 2014.

[19] M. Stevanovic and T. Stecenko, "Mechanical behaviour of carbon and glass hybrid fiber reinforced polyester composites," *Journal of Materials Science,* vol. 27, pp. 941-946, 1992.

[20] C. Dong and I. Davies, "Flexural properties of glass and carbon fiber reinforced epoxy hybrid composites," *Journal of Materials: Design and Application,* vol. 227, no. 4, pp. 308-317, 2012.

[21] R. Akkerman, "Laminate mechanics for balanced woven fabrics," *Composites: Part B,* vol. 37, no. 2-3, pp. 108-116, 2006.

[22] S. Tsai and N. Pagano, "Invariant properties of composite materials," Technomic Publishing Co, Lancaster, PA, 1968.

[23] N. Pagano and B. P. Pipes, "Some observations on the interlaminar strength of composite laminates," *International Journal of Mechanical Sciences,* vol. 15, no. 8, pp. 679-686, 1973.

[24] R. H. Martin, "Delamination Failure in a unidirectional curved composite laminate," National Aeronautics and Space Adminstration, Hampton, VA, 1990.

[25] F.-K. Chang and G. Springer, "The strengths of fiber reinforced composite bends," *Journal of Composite Materials,* vol. 20, no. 1, pp. 30-45, 1986.

[26] W. Ko and R. Jackson, "Multilayer Theory for Delaminations analysis of a composite curved bar subjected to end forces and end moments," National Aeronautics and Space Administration, Washington, DC, 1989.

[27] L. Hart-Smith, "Bolted joints in graphite-epoxy composites," National Aeronautics and Space Administration, Washington, DC, 1976.

[28] T. Collins, "The strength of bolted joints in multi-directional cfrp laminates," *Composites,* vol. 8, no. 1, pp. 43-55, 1977.

[29] H.-J. Park, "Effects of stacking sequence and clamping force on the bearing strengths of mechanically fastened joints in composite laminates," *Composite structures,* vol. 53, no. 2, pp. 213-221, 2001.

[30] N. Fleck, "Compressive Failure of fiber composites," *Advances in applied mechanics,* vol. 33, pp. 43-113, 1997.

[31] C. Sun and P. Wu, "Bearing failure in pin contact of composite laminates," *American institute of Aeronautics and Astronautics,* vol. 36, no. 11, pp. 2124-2129, 1998.

[32] P. Camanho and M. Lambert, "A design methodology for mechanically fastened joints in laminated composite materials," *Composites Science and Technology,* vol. 36, pp. 3004-3020, 2006.

[33] P. Camanho and F. Matthews, "A progressive damage model for mechanicall fastened joints in composite laminates," *Journal of composite materials* , vol. 33, no. 24, pp. 2248-2281, 1999.

[34] B. Vieille, J. Aucher and l. Taleb, "Woven ply thermoplastic laminates under severe conditions: Notched laminates and bolted joints," *Composites:Part B,* vol. 42, pp. 341-349, 2011.

[35] F. Matthews, A. Roshan and L. Phillips, "The bolt bearing strength of glass/carbon hybrid composites," *Composites,* vol. 13, no. 3, pp. 225-227, 1982.

[36] L. Nohara, E. Nohara, A. Moura, J. Goncalves, M. Costa and M. Rezende, "Study of crystallization behaviour of polyphenylene sulfide," *Polimeros,* vol. 16, no. 2, pp. 104-110, 2006.

[37] S. Beland, High performance thermoplastic resins and their composites, New Jersey: Noyes, 1990.

[38] H. Peidong, B. Joe, M. Price, S. Buchanan and A. Murphy, "Experiemental investigation of thermoforming carbon fiber-reinforced polyphylene sulfide composites," *Journal Of Thermoplastic Composite Materials,* vol. 28, no. 4, pp. 529-547, 2015.

[39] EN2562, "Flexural test parallel to the fiber direction," European Commttee for Standardization, 1997.

[40] S. Lekhnitskii, "Anisotropic Plates," Gordon and Breach Science Publisher, New York, 1968.

[41] G. Kardomateas and R. Carlson, "A micromechanical model for the fiber bridging of macro cracks in composite plates," *Journal of applied mechanics*, vol. 63, no. 1, pp. 225-233, 1996.